國 立 交 通 大 學

電子工程學系電子研究所碩士班

碩 士 論 文

利用光激發於結合光子晶體的類型二量子井之研究

Study of Type II QW with photonic crystal structure by optical pumping

研 究 生：林俊豪

指導教授：李建平 教授

中 華 民 國 九 十 八 年 十 月

利用光激發於結合光子晶體的類型二量子井之研究

Study of Type II QW with photonic crystal structure by optical pumping

研 究 生：林俊豪　　　　　　　　　　Student：Chun-Hao Lin

指導教授：李建平　　　　　　　　　　Advisor：Dr. Chien-Ping Lee

國 立 交 通 大 學

電子工程學系電子研究所碩士班

碩 士 論 文

A Thesis
Submitted to Department of Electronic Engineering and
Institute of Electronics
College of Electrical and Computer Engineering
National Chiao Tung University
in partial Fulfillment of the Requirements
for the Degree of
Master
in Electronic Engineering
June 2009
Hsinchu, Taiwan, Republic of China

中華民國九十八年十月

利用光激發於結合光子晶體的類型二量子井之研究

學生:林俊豪　　　　　　　　指導教授:李建平博士

國立交通大學

電子工程學系　電子研究所碩士班

摘要

　　本篇論文為結合光子晶體與第二型量子井之研究。第二型量子井因其介面放光機制,發光效率較小,但藉由光子晶體共振腔結構,可耦合出頻寬窄且強度高的共振模態。利用電子束微影術,乾式蝕刻及選擇性濕式蝕刻成功製作出光子晶體共振腔結構,且此透過適當設計的光子晶體共振腔具有高品質因子特性。實驗中,在溫度 77K 下,我們利用顯微光激發螢光量測系統成功得到具有高達 15170 品質因子的單模共振模態。從以知文獻中,這是在結合光子晶體共振腔結構的第二型量子井材料中,第一次量測到具有高達 10^4 級數的品質因子。

Study of Type II QW with photonic crystal structure by optical pumping

Student: Chun-Hao Lin   Advisor: Dr. Chien-Ping Lee

Department of Electronics Engineering & Institue of Electronics

National Chiao Tung University

Abstract
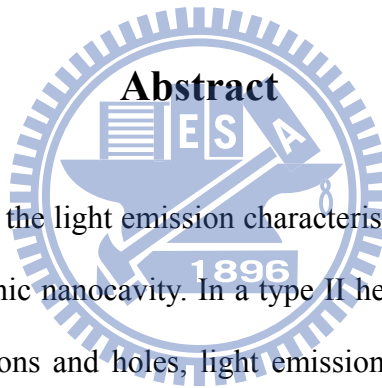
In this research, we studied the light emission characteristics of GaAs/GaAsSb type II heterostructures in a photonic nanocavity. In a type II heterostructure, because of the spatial separation of electrons and holes, light emission efficiency is typically very small. However, by coupling the emission peak with the cavity mode, we are able to obtain sharp and intense emission from the type II heterostructure. The nanocavity was fabricated in a suspended thin film photonic crystal. The defect cavity was specially designed to have the desired cavity mode with a high Q value. E-beam lithography, dry etching and selective wet chemical etching were used to fabricate the nanocavity. The emission spectrum was measured by a micro-photoluminescence system using optical pumping. At 77K, an emission peak at 1004nm with a very high Q factor of 15170 was obtained. To our knowledge, this is the first time that a type-II heterostructure emission was coupled to a photonic nanocavity with a very sharp emission and a high Q value.

Acknowledgement(誌謝)

Contents

List of Figures

Chapter 1   Introduction

Recently, optical communication has been an important role in the application of internet and signal transmission. However, it is a challenge on how to maintain signal integrity and reduce noise distortion after long-distance transmission. Since some specified wavelengths, like 1.3um and 1.5um, in near infrared region (NIR) possess less dispersion and attenuation characteristics in fiber transmission, it's a good choice for us to develop laser sources at these wavelengths. [1]

In type I heterostructures, illustrated in Fig.1.1(a), the band gap of one material overlaps that of the other so that both electrons and holes are confined in the lower-band-gap material in these heterostructure. For Type II materials, Fig.1.1(b), both the conduction-band edge and the valence-band edge of one material being lower than the corresponding band edges of the other material, electrons are confined in one material, while holes are confined in the other material[2]. That is, electrons and holes are combined at the interface to emit photon and this mechanism is expected to be suitable for photonic devices with longer wavelength.

Photonic crystal concepts are first introduced by prof. Eli Yablonovitch and prof. Sajeev John in 1987.[3][4] Since photonic crystal micro-cavity, created by a point defect, has small excited mode volume and high quality factor value. It's promising for laser source with low threshold current. In 1999, O.Painter et al first successfully realize photonic crystal laser. [5] Subsequently all kinds of cavity laser are designed, like L-3 structure by S.Noda[6], point-shift structure by T.Baba[7], and so on.

Nowadays, edge-emitting lasers with type II materials have been achieved [8-11], as well as type II surface-emitting lasers [12-13]. Nevertheless, most surface-emitting lasers researches focus on DBR structure. Here combined type II materials with photonic crystal micro-cavity are first studied.

In this thesis we first introduce basic principles of Type II materials and photonic crystal individually in chapter 2. In chapter 3, the fabrication process and measurement system are described. Chapter 4 is devoted to discuss the simulation and measurement results. We obtain the quality factor value by 3D FDTD (finite difference time domain) calculation. Finally, we conclude this thesis in chapter 5 with hope for single mode laser by electric pumping.
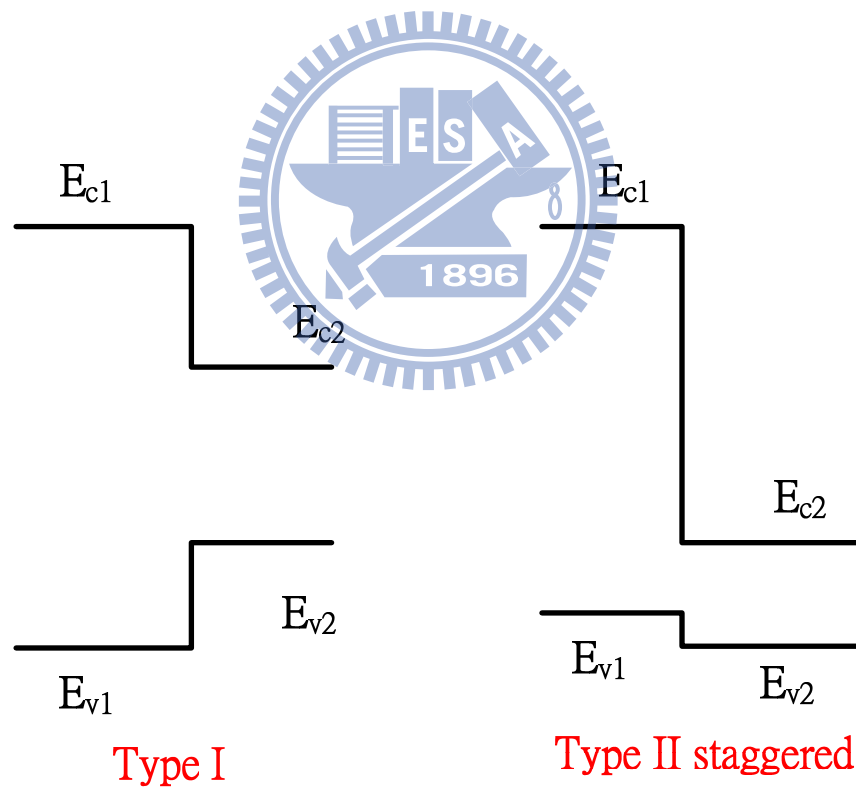
Fig.1.1 Band alignments in heterojunctions. (a) Type I heterostructure. (b)Type II-staggered heterostructure.

Chapter 2 Fundamental theorem of Type II quantum well and photonic crystal cavity structure

2.1 Type II quantum well blue-shift characteristic

Blue-shift phenomenon is ascribed to band bending effect due to spatial separation of photo-generated electrons and holes [14][15]. In our research, we use GaAsSb/GaAs quantum well. When we add external optical pumping power, the electrons and holes may accumulate on two sides of the GaAsSb/GaAs interfaces. Fig.2.1 shows the band diagram (solid line) and wave function (dash line) for a type-II quantum well system [16]. The separation causing band bending to form triangular well near the interface is evident. The more incident power we add, the larger energy difference between electron ground state and the hole ground state is, which results from much more coulombic interaction and the steeper triangular well. That is, the total energy increases as incident optical power rises. Besides, the ground state energy in the triangular well has been proven proportional to third root of external incident power [17]. Therefore, we observe blue-shift occurrence with increasing power and the central wavelength is linear to the cubic root of the incident power.
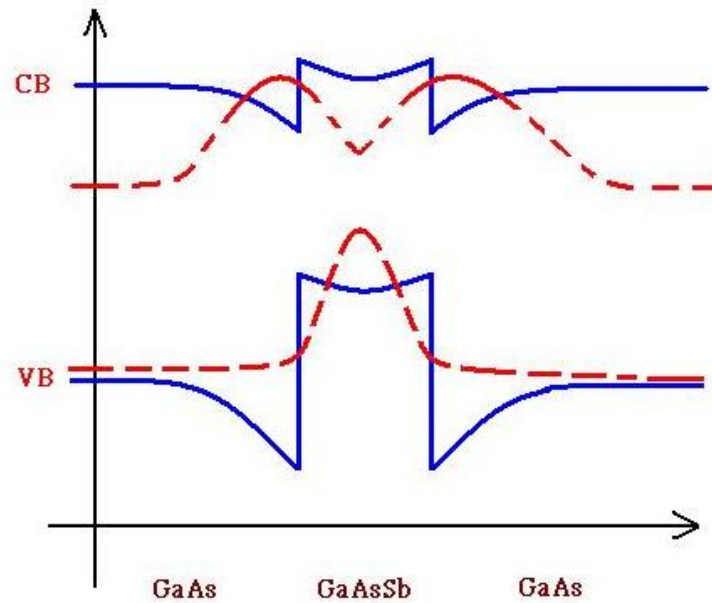
Fig.2.1 Band diagram (solid line) and wave function (dash line)

of type II quantum well system

2.2　Photonic crystal fundamental theorem

Photonic crystal consists of macroscopic media with periodic dielectric constants, or, equally, a periodic refraction index. Similar to electron, photon has band gap also, due to its refraction and reflection behaviors. We can design appropriate photonic crystal with photonic band gaps to prevent light with particular frequencies from propagating in certain directions.

Next, we analyze photonic crystal basic physical principle by Maxwell equations. In the following assumption: firstly, there are no free charges or currents in the structure. Secondly, we assume dielectric constants are real and positive which represents the material are transparent. Finally, dielectric

constants are independent of frequency. Maxwell equation could be written in the form:

$$\nabla \cdot H(r,t)=0 \tag{1}$$

$$\nabla \times E(r,t)+\mu_0\frac{\partial H(r,t)}{\partial t}=0 \tag{2}$$

$$\nabla \cdot [\varepsilon(r)E(r,t)]=0 \tag{3}$$

$$\nabla \times H(r,t)-\varepsilon_0\varepsilon(r)\frac{\partial E(r,t)}{\partial t}=0 \tag{4}$$

where r is position vector, ε_0 and μ_0 are permittivity and permeability, and E and H are electric field and magnetic field individually.

Although E and H are complex functions with time and space, we can separate the time dependence from the space dependence since the equations are linear. Therefore, we can write fields as harmonic modes which vary sinusoidally with time.

$$H(r,t)=H(r)e^{-iwt} \tag{5}$$

$$E(r,t)=E(r)e^{-iwt} \tag{6}$$

Putting Eq.(5) and Eq.(6) back to (1)-(4),we get

$$\nabla \cdot H(r)=0 \tag{7}$$

$$\nabla \cdot [\varepsilon(r)E(r)]=0 \tag{8}$$

$$\nabla \times E(r)-i\omega\mu_0 H(r)=0 \tag{9}$$

$$\nabla \times H(r)+i\omega\varepsilon_o\varepsilon(r)E(r)=0 \tag{10}$$

The first two equations have physical representation: no point sources and sinks of displacement and magnetic field are in the media. We also can rewrite the last two equations into

$$\nabla \times (\frac{1}{\varepsilon(r)} \nabla \times H(r)) = (\frac{\omega}{c})^2 H(r) \tag{11}$$

with $c = \dfrac{1}{\sqrt{\varepsilon_0 \mu_0}}$,c is the vacuum speed of light. Obviously Equation (11) is eigenfunction, we can use operator $\hat{\Theta}$ instead of $\nabla \times (\dfrac{1}{\varepsilon(r)} \nabla \times$ for convenience. $\hat{\Theta}$ is also Hermitian operator which has some properties, for example, with orthogonality and real eigenvalues.

2.3 Two dimensional (2D) photonic crystal cavity slab characteristics

Fig.2.2 is the conventional 2D photonic crystal (PC) hole slab [17]. There are some relevant symmetries, such as discrete translational symmetry, rotation symmetry, mirror symmetry, etc, in 2D PC slab. With discrete translational symmetry in two directions (x and y), the in-plane wave vector $k_{\parallel}$=(k_x, k_y) is conserved. Also from mirror symmetry we can distinguish the modes for k_z=0 into two polarizations: TE-like and TM-like. Fig.2.3 [18] is the TE-like band diagram of hole slab.

2D PC slab can inhibit emission to the in-plane spontaneous emission due to photonic band gap effect [19]. At the same time, excited carriers which were primarily distributed to in-plane emission become redistributed for vertical emission. We can classify total spontaneous emission rate as three parts:

$$R_{total} = R_{slab} + R_{vertical} + R_{non-radiation} \tag{12}$$

where R_{slab} and $R_{vertical}$ indicate spontaneous emission rate for in-plane direction and vertical direction respectively[20]. R_{slab} satisfies the total internal reflection at the interface between air and semiconductor, but $R_{vertical}$ doesn't. $R_{non-radiation}$ is the non-radiation recombination rate which is dominated by surface recombination mechanism. Without photonic crystal pattern, R_{slab} is much higher than $R_{vertical}$ because of high index ratio of semiconductor and air. That is, most carriers are confined to in-plane emission due to total internal reflection. After adding photonic crystal structure with adequate frequency range, however, in-plane emission is not allowed anymore. Therefore, we can think of R_{slab} as zero, and then total emission rate becomes

$$R_{total} = R_{vertical} + R_{non-radiation} \tag{13}$$

From Fig.2.4 [21], when the wavelength is located within photonic band gap, the detected intensity corresponding to vertical emission is more enhanced compared to the one which the wavelength is outside photonic band gap. Simultaneously, emission lifetime is longer because in-plane emission is restricted and then only vertical emission is permitted to emission.

When introducing point defect (cavity) into 2D PC slab, it produces localized modes which are leaky resonances with vertical radiation loss due to the presence of light cone. Here we briefly account for quality factor, Q. Q is dimensionless lifetime and 1/Q is the fractional bandwidth of the resonance. The definition of Q is $2\pi \frac{\text{Energy stored}}{\text{Energy lost in one oscillation}}$, or $Q = \frac{2\pi v}{\alpha}$ where v is resonant frequency of cavity and α is decay constant of stored energy,

$U(t) = U_0 \exp(-\alpha t)$, or $Q = \dfrac{\lambda_0}{\Delta\lambda_{FWHM}}$ where λ_0 is central wavelength of cavity

mode and $\Delta\lambda_{FWHM}$ is full-width at half maximum of the resonant peak. Besides, if there are more than one decay mechanisms in the cavity, we can interpret total quality factor in each quality factor with own mechanism.

$$\frac{1}{Q_{total}} = \sum_i \frac{1}{Q_i} \tag{14}$$

In general, there are two mechanisms in the cavity. One is the light decay into parallel slab (Q_{slab}), the other is to surrounding air ($Q_{vertical}$). That is,

$$\frac{1}{Q_{total}} = \frac{1}{Q_{slab}} + \frac{1}{Q_{vertical}} \tag{15}$$

Normally Q_{slab} increases exponentially with the number of holes of each side, so Q_{slab} can be regarded as infinity, and then Q_{total} is nearly equal to $Q_{vertical}$. Since high Q is required in many applications, such as low-threshold lasers, how to increase quality factor becomes a crucial issue. Basically there are two mechanisms: Delocalization and Cancellation. Delocalization means we make the defect weaker by reducing the dielectric contrast relative to the rest of the slab or, alternatively, changing neighboring holes shapes and positions. The reason to increase Q is the more delocalized it is in shape, the more localized its Fourier transform can be [5]. This allows most of the Fourier components to lie inside the light cone and not radiate, as shown in Fig.2.5. Changing neighboring holes, however, increases the mode volume. According to Purcell effect, the rate of spontaneous emission is proportional to Q/V in the resonant cavity, so the performance of laser or LED is dependent of mode volume. Consequently there is an optimal situation of changing neighboring holes

(either shape or position). On the other hand, we can describe cancellation as the dominant component of the radiation is eliminated by a forced balance of scattered fields with opposite signs. Generally the field can be expressed by a multiple expansion and higher Q could be obtained if the dipole mode vanishes [21]. The reason is the positive and negative amplitude of dipole mode electric field are not symmetric and then leads to vertical radiation is not efficiently confined and quality factor is reduced owing to vertical loss. Fig.2.6 shows the vertical confinement of dipole and hexapole individually.
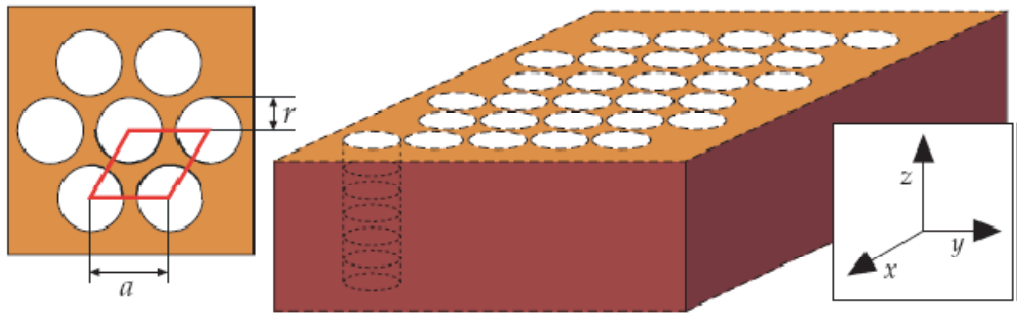
Fig.2.2 Conventional 2D photonic crystal hole slab [2-4]
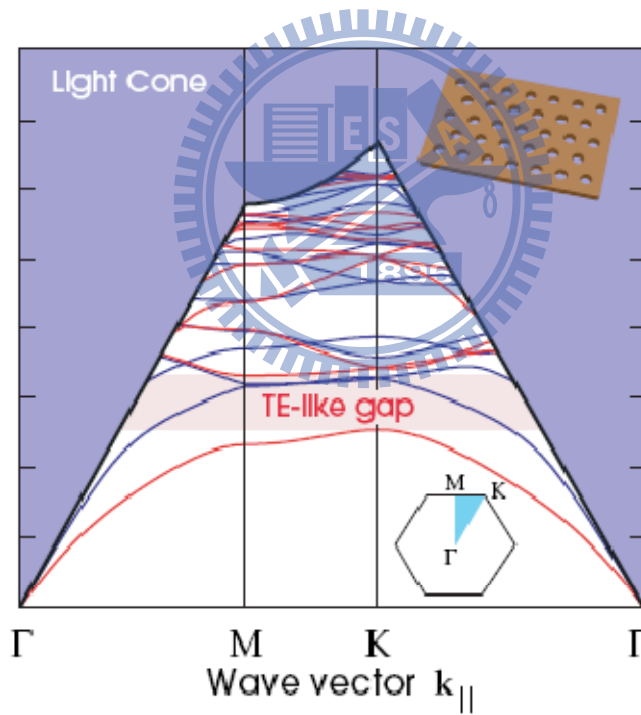
Fig.2.3 TE-like band diagram of 2D photonic crystal hole slab [2-5]
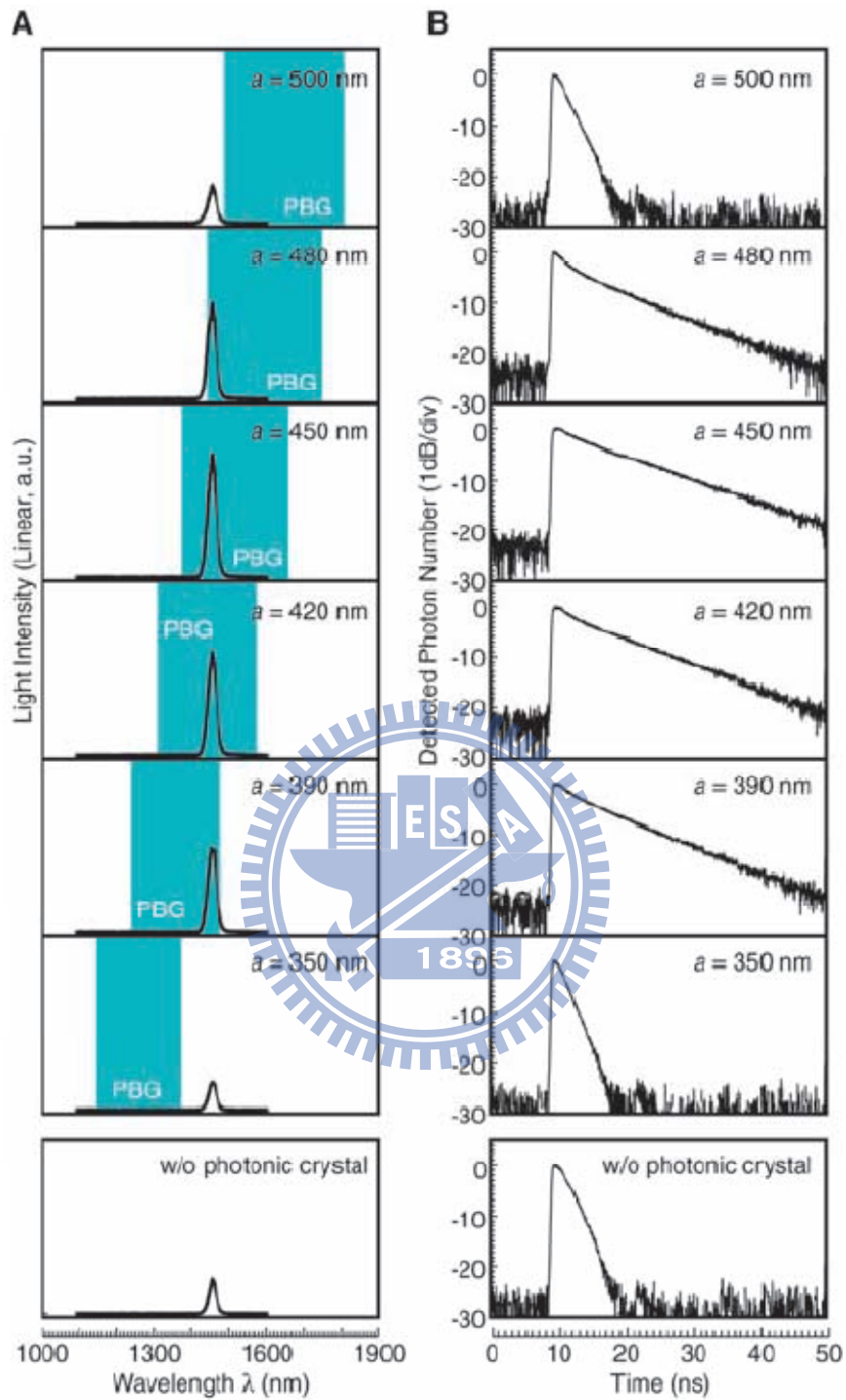
Fig.2.4 Change of emission intensity and carrier lifetime after adding photonic crystal structure [21]
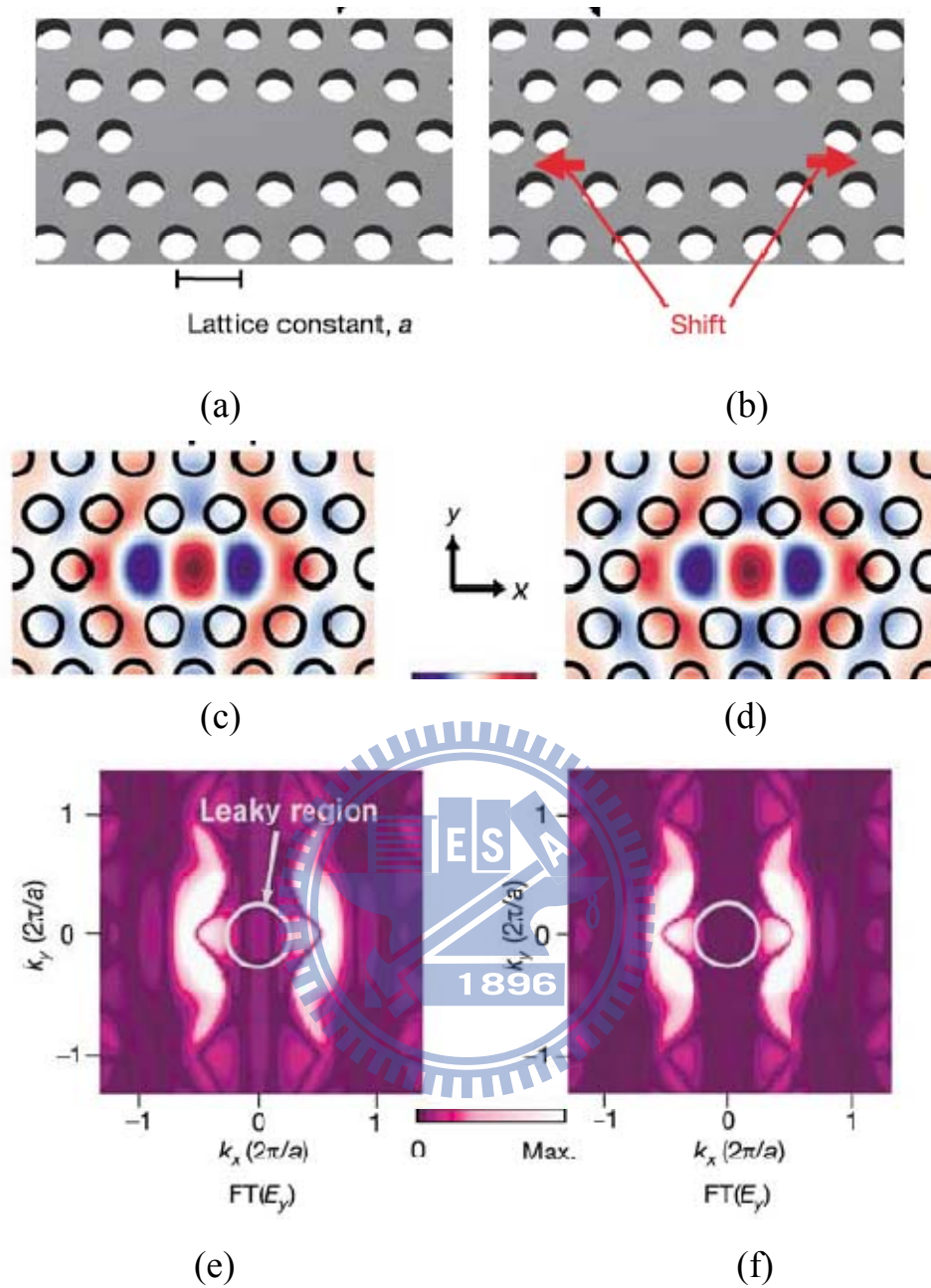
Fig2.5 Design of high Q cavity

(a) Basic cavity without shifting neighboring holes

(b) Modified cavity with shifting two nearest holes

(c) The electric field of the fundamental mode of basic cavity

(d) The electric field of the fundamental mode of modified cavity

(e) The Fourier transform of basic cavity electric field

(f) The Fourier transform of modified cavity electric field
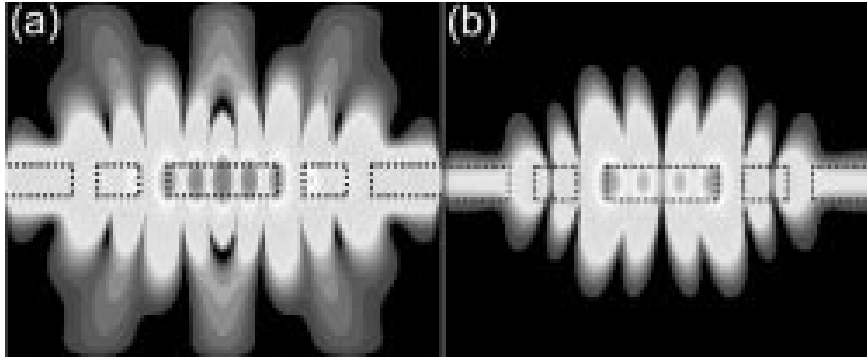
Fig.2.6 Comparison of vertical confinement of (a) dipole mode and (b)

hexapole mode individually

2.4 Calculation of effective refractive index

The purpose of calculating effective refractive index (n_{eff}) is that we can

use 2D simulation instead of time-consuming 3D simulation.

As well known, it's very crucial to design the appropriate thickness of

membrane when electromagnetic wave is confined in resonant cavity. If it is

too thick, the resonant mode is not allowed only as single mode. On the

contrary, if it's too thin, effective refractive index approaches surrounding

material refractive index (air), and then the probability of total internal

reflection is significantly reduced to worsen the vertical confinement.

Therefore, we evaluate the membrane thickness by solving electric field

distribution.

As shown in Fig.2.7, middle layer (b layer) is membrane structure (active

region), and upper layer (a layer) is air region, as well as lower layer (c layer).

Since electromagnetic wave is confined in membrane region, like standing

wave, electric field in membrane is cosine wave (even mode) and electric field in air region is evanescent wave form. Here we neglect sine wave (odd mode) since the membrane thickness is so thin that odd mode has slight interaction with active medium. We can describe electric distribution as

In membrane region: $\quad E(z) = E_b \cos(h_2 z + \phi)$ (16)

In upper air region: $\quad E(z) = E_a \exp[-\gamma_1 (z - d/2)]$ (17)

In lower air region: $\quad E(z) = E_c \exp[\gamma_3 (z + d/2)]$ (18)

According to continuous of electric field and differential electric filed, we can write down the distribution form at the interface, z=d/2, of upper layer and membrane.

$$E_a = E_b \cos(h_2 d/2 + \phi)$$ (19)

$$-\gamma_1 E_a = -h_2 E_b \sin(h_2 d/2 + \phi)$$ (20)

At the same time, the electric field distribution at the interface, z= -d/2, of membrane and lower layer.

$$E_c = E_b \cos(-h_2 d/2 + \phi)$$ (21)

$$\gamma_3 E_c = -h_2 E_b \sin(-h_2 d/2 + \phi)$$ (22)

After calculation, we can get the eigenvalue equations:

$$\tan(h_2 d) = \frac{h_2 (\gamma_1 + \gamma_3)}{h_2^2 - \gamma_1 \gamma_3}$$ (23)

and

$$\tan(2\phi) = \frac{h_1 (\gamma_2 + \gamma_3)}{h_1^2 + \gamma_2 \gamma_3}$$ (24)

where $\quad h_2^2 = k_2^2 - \beta^2$ (25)

$$\gamma_1^2 = \beta^2 - k_1^2 \qquad (26)$$

$$\gamma_3^2 = \beta^2 - k_3^2 \qquad (27)$$

where β is the propagation constant and $n_\beta = \dfrac{c\beta}{\omega} = \dfrac{\beta\lambda}{2\pi}$ is the effective refractive index.

In our structure, it's a symmetric slab, n1=n3=1 and $\gamma_1 = \gamma_3$. Then Eq. (24) becomes $\tan(2\phi) = 0$ and $\phi = m\pi, m = 0,1,2,...$ for even mode. Besides, Eq. (23) can be transformed to

$$\tan(\frac{h_2 d}{2}) = \frac{\gamma_1}{h_2} = \frac{\sqrt{V^2 - h_2^2 d^2}}{h_2 d}$$

(28)

Here we introduce a parameter: the normalized frequency and waveguide thickness, also called as the V number. The definition is

$$V = \frac{2\pi}{\lambda} d \sqrt{n_2^2 - n_3^2} \qquad (29)$$

and the mode number is equal to

$$M = [\frac{V}{\pi}]_{int} \qquad (30)$$

Since we require the resonant cavity is operated only as single mode, V_{max} is π and then the membrane width, d, could be determined by Eq. (29) with known λ, n_2 and n_3. After calculation we get $d = 154 nm$. Here our membrane width equal to170nm is designed for safety because our structure doesn't consist of solo GaAs but GaAs mixed with air hole, which means refractive index is less than 3.42.

Next h_2 is decided by solving Eq. (28). Since Eq. (28) is a transcendental equation, we have to calculate it graphically. Fig.2.8 shows the graphic solution

for Eq. (28). From Fig.2.8, the cross point is located at $h_2 d = 1.876$, that is $h_2 = 12.181$. Once h_2 is known, β and n_β could be solved subsequently. Here we obtain β and n_β are 17.55 and 2.8 respectively. That is, in 2D simulation, the structure, included with two-side air layer and middle membrane, has effective refractive index, 2.8, but not bulk index, 3.42.
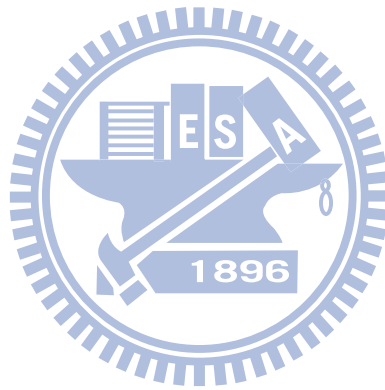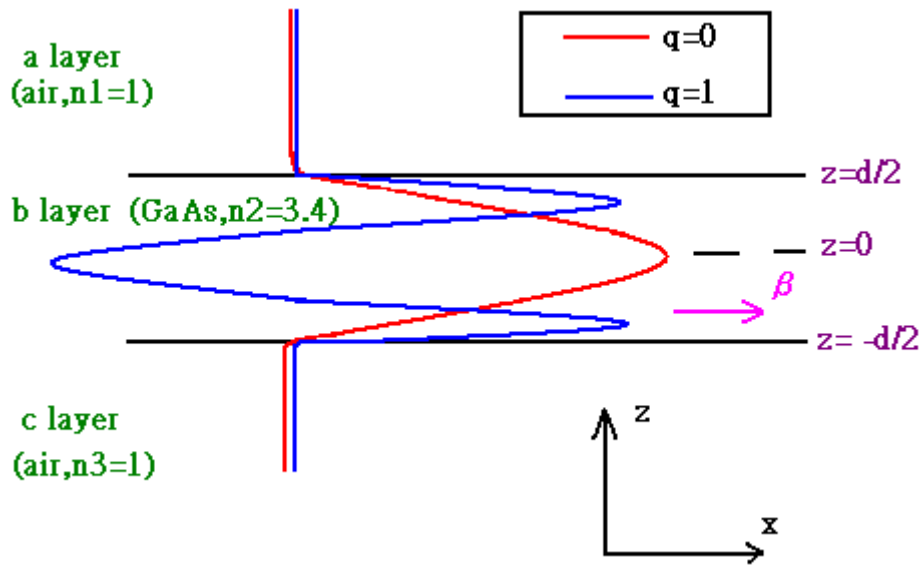
Fig.2.7 Electric field distribution of three layer structure
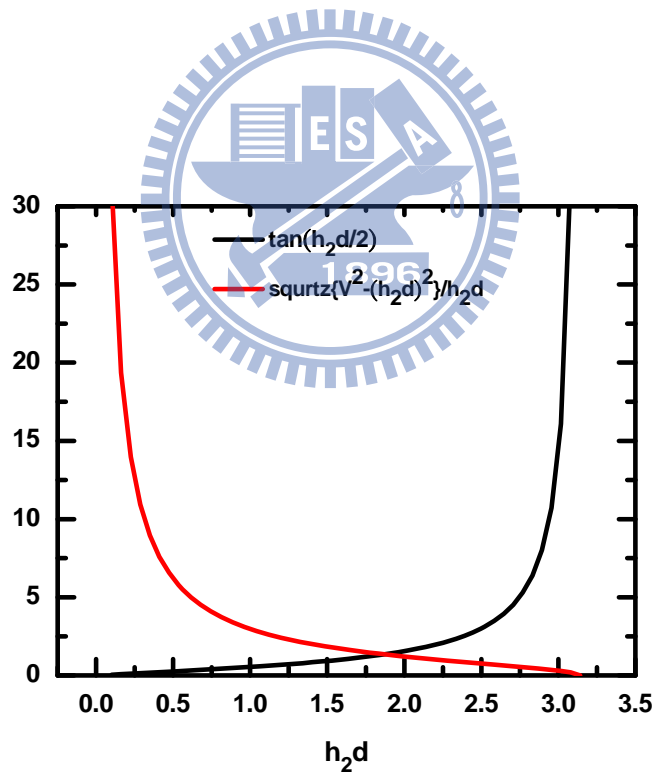
Fig.2.8 Graphic solution for the eigenvalues of a symmetric slab of V=π

Chapter 3 Fabrication process and measurement system

3.1 GaAs-GaAs$_{0.7}$Sb$_{0.3}$ Type II tri-layer quantum well(QW) structure

The structure, as shown in Fig. 3-1, is based on n$^+$ GaAs substrate covered with sacrificed layer, Al$_{0.7}$Ga$_{0.3}$As, with thickness 1.2μm. This layer thickness is larger than ground state emission wavelength, 1μm (FWHM is 54nm), as shown in the inset of Fig.3-2, so as to prevent the light absorption due to substrate. The active region, total width 170nm, comprises of three GaAs-GaAs$_{0.7}$Sb$_{0.3}$ type II quantum well pairs, sandwiched with 50nm GaAs as wave-guided layer. As mention earlier, Type II QW has blue-shift and the peak wavelength proportional to the cubic root of the incident power characteristics. Here photon luminescence with six different incident powers are measured, shown in Fig.3.3, the central wavelength for the smallest incident power,6 μW, is located at 1006 nm. Then the central wavelength has blue shift phenomenon as incident power increases. For the largest incident power, 550 μW, the central wavelength moves to 987nm. Next, peak energy versus the third root of incident power is plotted and the linear relationship between peak energy and the cubic root of incident power, Fig3.4, is observed. According to these consequences, we confirm our structure consists of Type II materials definitely.
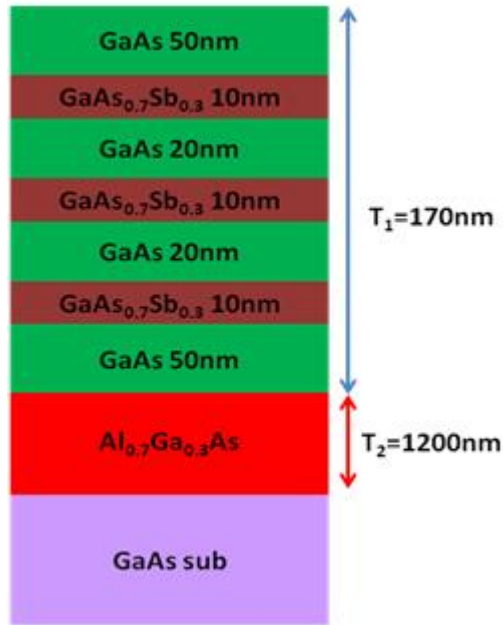
Fig.3.1 GaAs-GaAs$_{0.7}$Sb$_{0.3}$ Type II tri-layer QW structure
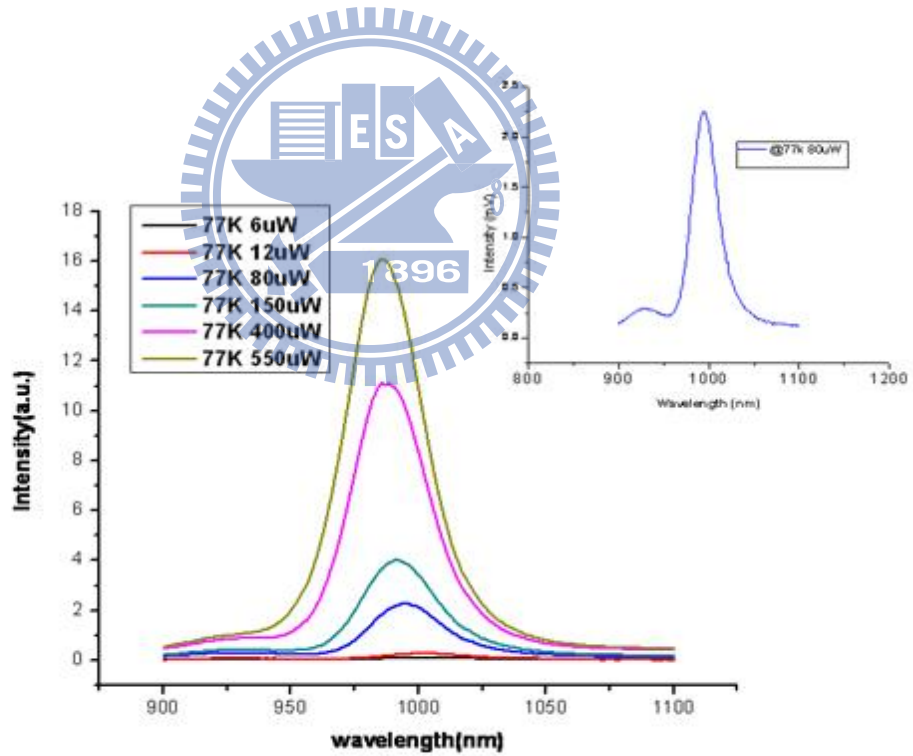
Fig.3.2 PL spectrum-Type II QW blue-shift character (The inset shows the central wavelength peak is approximately located at 1um with low incident power (FWHM is 54nm))
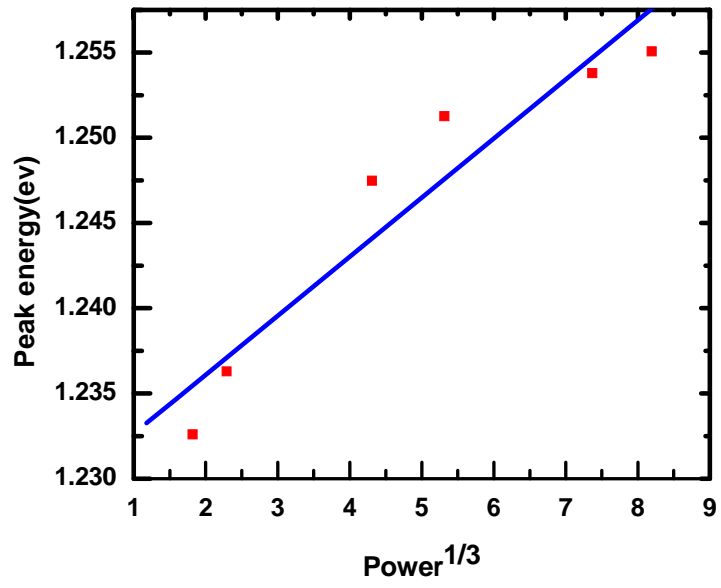
Fig.3.3 Dependence of peak energy on the cubic root of incident power
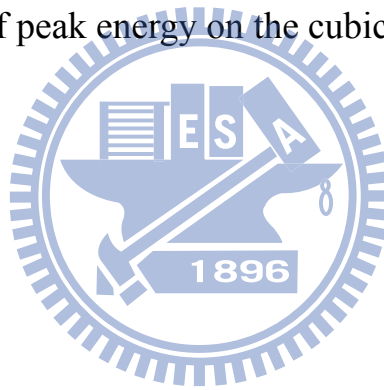
3.2 Photonic crystal fabrication

Type II QW membrane structure is fabricated as follows: 2500-Å-thick 5% poly (methylmethachrolyne)(PMMA) is coated on the top surface of SiNx layer,3000 Å ,which is coated on the top of wafer by PECVD and used as ion-etching buffer layer since PMMA is not rigid enough to sustain the bombardment from ion-etching plasma.

The hexagonal lattice photonic crystal with micro-cavity patterns are written by e-beam lithography. Here the square areas, shown in Fig.3.6, at both sides of photonic crystal patterns are designed as 'wet etching window' intentionally in order to make wet etching process at last step successfully. Due to proximity effect, the phenomenon that exposure dose distribution, and hence the developed pattern, is wider than the scanned pattern, because of the interactions of the primary beam electrons with the resist and substrate, the dose value of wet etching window is smaller than that of photonic crystal pattern since the area of wet etching window is much larger than that of photonic crystal pattern. After developing process, dry etching process is continued. First, we transfer pattern from PMMA to SiN_x by CHF_3 and O_2 gas for four minutes, and then PMMA is removed by O_2 plasma since the chemical property of PMMA is changed during the dry-etching process. Secondly, $SiCl_4$/Ar gas are used in order to transfer pattern from SiN_x to the active region, GaAsSb/GaAs layer, the etching time is one minute and ten seconds and then SiN_x layer is removed by CHF_3/O_2 gas again. It's important that each etching time should be long enough to etch each layer completely; otherwise, photonic crystal pattern can't transfer to bottom layer successfully.

Finally, diluted HF solution, H_2O/HF volume ratio 50[22][23], separates the slab containing QWs from GaAs substrate by etching $Al_{0.7}Ga_{0.3}As$ sacrificed layer. The purpose of wet etching window is not only to increase etching rate due to larger area where diluted HF solution can pour into, but also to be a channel that the product after $Al_{0.7}Ga_{0.3}As$ and diluted HF reaction can flow away. Besides, because $Al_{0.7}Ga_{0.3}As$ is easily oxidized, wet etching process should be operated as soon as possible after dry etching process is finished. Here wet etching process time is about seventeen minutes. Next the pattern is heated by hot plate to remove remaining solution. Since photonic crystal pattern is now suspended in midair, that is, the structure is fragile; hot plate is used but not air gun, which may make damage to our sample. 2-D photonic crystal membrane structure is then completed. The total process flow is shown in Fig.3.4. Fig.3.5 and Fig.3.6 show SEM picture of cross view and top view of 2D membrane individually. From Fig.3.5 (a), $Al_{0.7}Ga_{0.3}As$ sacrificed layer is apparently removed and micro-cavity region is still conserved after total process, shown in Fig.3.5 (b). In Fig.3.6, the array of photonic crystal pattern is exhibited to illustrate our high experimental yield.
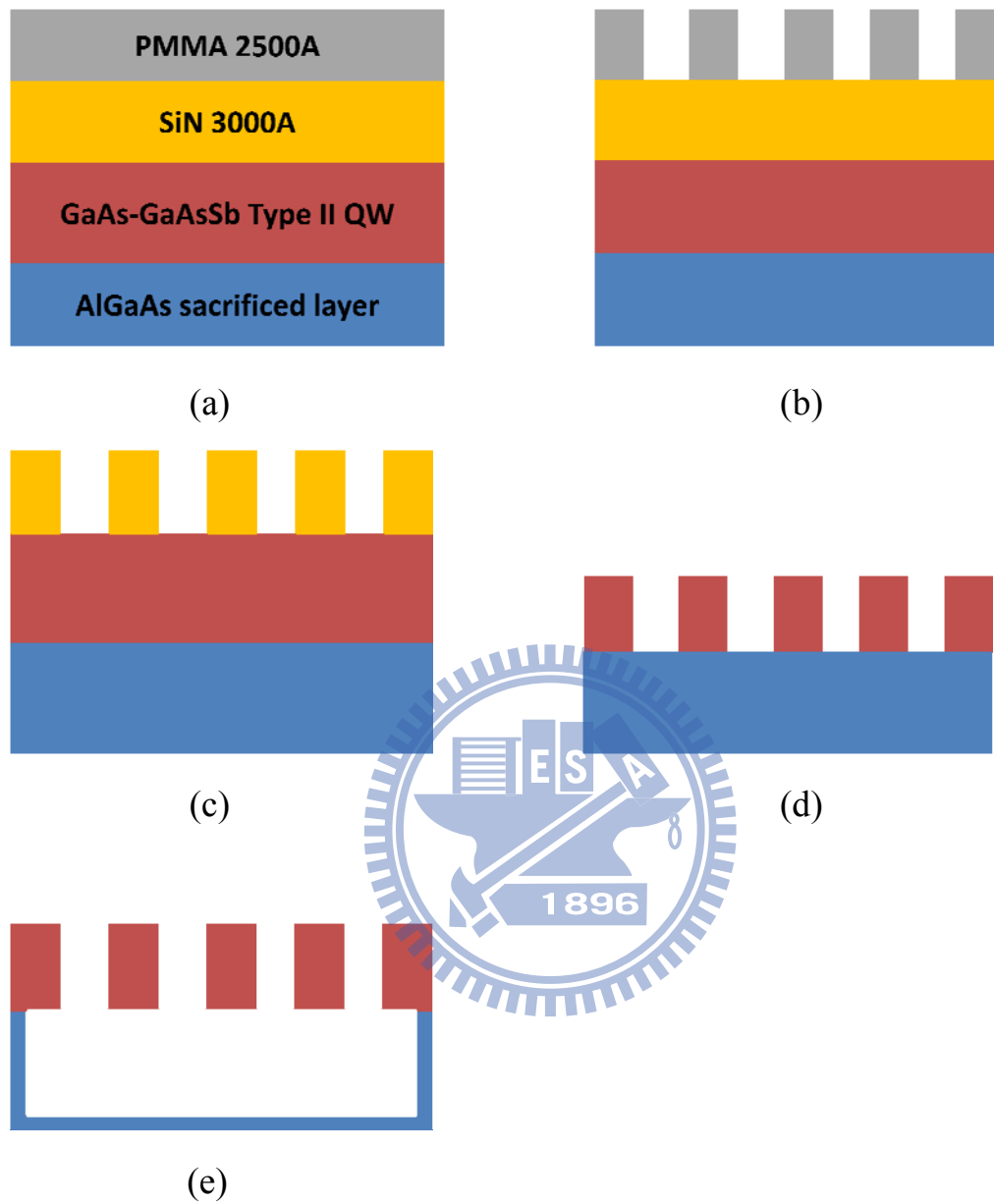
Fig.3.4 Fabrication process flow:

(a) The sample is coated by SiN and subsequently by PMMA

(b) Developing process

(c) Transferring pattern from PMMA to SiN

(d) Transferring pattern from SiN to GaAs

(e) Remove sacrificed layer by DHF

(a)   (b)
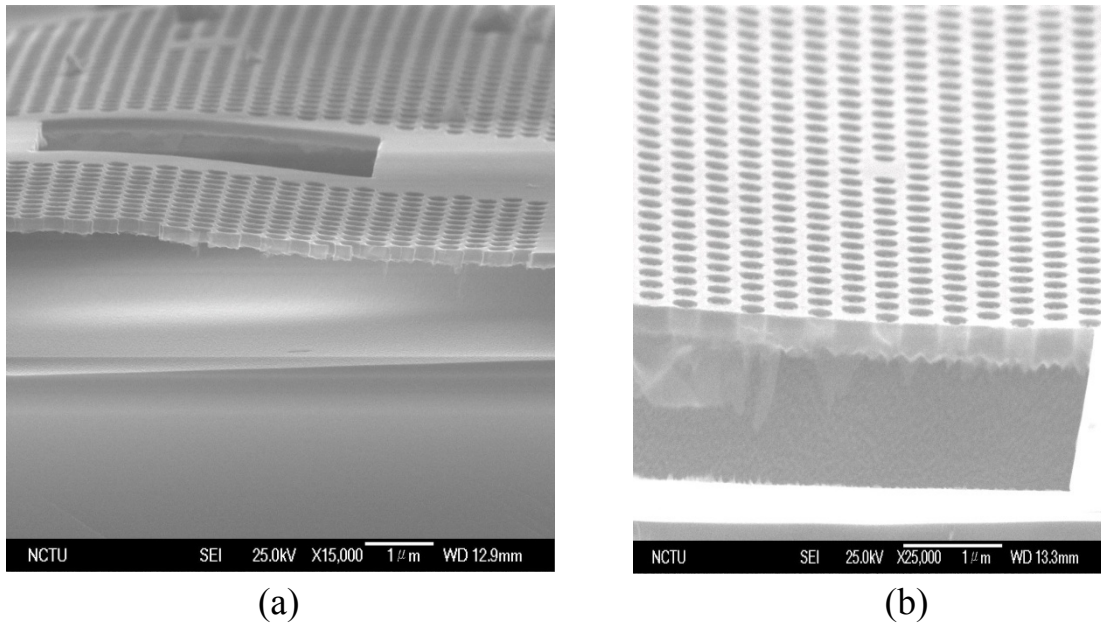
Fig.3.5 Cross view of 2D photonic crystal membrane
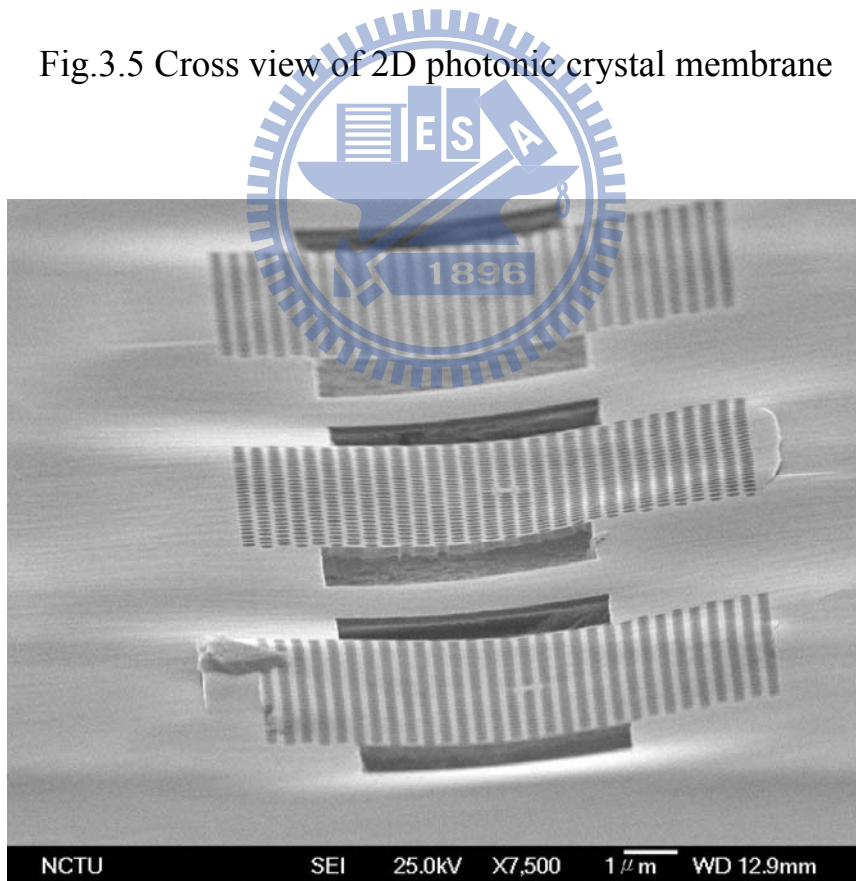
Fig.3-6 Top view of 2D photonic crystal membrane

3.3 Micro photoluminescence (μ-PL) measurement system

At beginning, we introduce photoluminescence principle shortly. When adding incident power, larger than band gap of semiconductor, from laser source which provides sufficient and stable power to excite appropriate signal, electrons in valence band are excited to conduction band and holes are left in valence band at the same time, and then most electrons in the conduction band release energy gradually by non-radiative recombination, such as phonon emission, Auger effect, until they arrive at the ground state of conduction band. Electrons and holes are recombined and emit a photon. Photoluminescence could be used to provide the information whether the sample epitaxy is good or not and verify the substance or structure of the sample.

Measurement system is shown in Fig.3.7. Using central wavelength 633nm continuous wave (CW) He-Ne laser with maximum average incident power 30W as optical pumping source, we focus this laser light on our sample by object lens. The spot diameter is about 2~3 μm. The sample is excited and then the emission fluorescence is detected by InGaAs detector, main response wavelength from 900nm to 1500nm, in the monochromator system. Here measurement temperature of the experiment is operated at 77K by liquid nitrogen cooling system since surface velocity of GaAs is $2*10^7$ cm/s, which lead to severe non-radiative recombination at room temperature.

Since photonic crystal micro-cavity area is only 1-2 μ m^2, high magnification object lens is needed to concentrate incident light on micro-cavity area. In our measurement system, co-focal microscope with

long-distance focus object lens which magnification is 100 is selected. In co-focal microscope, a laser beam passes through a light source aperture and then is focused by an object lens into a small focal volume on the surface of a sample. Emission photons from the sample excited by laser source are re-collected by the object lens. A beam splitter separates off some portion of the light into InGaAs detector. Here 633nm filter prevents laser light from entering the detector.
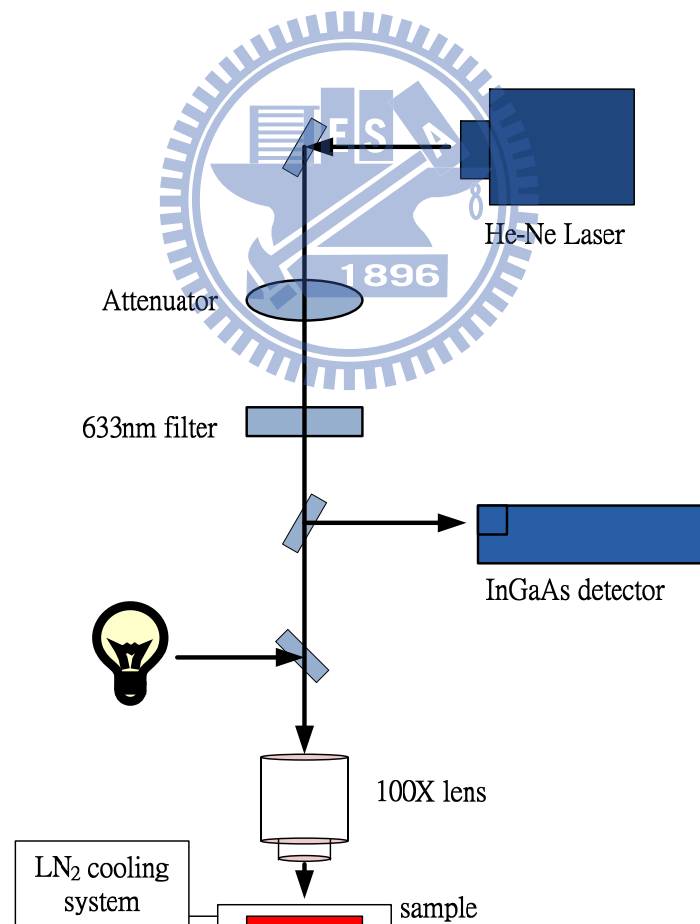
Fig.3.6 μ-PL measurement system

Chapter 4 Design of photonic crystal and simulation results

The methods to calculate photonic band gap and electromagnetic field distribution are 'Plane Wave Expansion method', 'Finite Difference Time Domain method', and 'Transfer Matrix method'. In our research, we use 'Plane Wave Expansion method' to calculate photonic band gap and 'FDTD method' to calculate resonant mode profile.

'Plane Wave Expansion method' calculate dispersion relations by periodic varied dielectric constants. According to Block's theorem, periodic varied dielectric constants could be expanded by Fourier transform and then band structure of photonic crystal could be calculated by solving Maxwell equations.

As well known, periodic dielectric constants expanded by Fourier transform can be written as

$$\frac{1}{\varepsilon(\vec{r})} = \sum U_{\vec{G}} e^{i(\vec{G}.\vec{r})} \tag{31}$$

where

$$U_{\vec{G}} = \frac{1}{\Lambda} \int_{\Lambda} \frac{1}{\varepsilon(\vec{r})} e^{-i(\vec{G}.\vec{r})} d\tau \tag{32}$$

Λ is unit lattice volume and $\vec{G}$ is reciprocal lattice vector.

Besides, the eigenfuction of periodic potential energy, $\varphi_k(\vec{r})$, can be expressed as the product of a plane-wave, $e^{i(\vec{k}.\vec{r})}$ and a periodic function of lattice constant, $u_k(\vec{r})$. That is,

$$\varphi_k(\vec{r}) = u_k(\vec{r}) e^{i(\vec{k}.\vec{r})} \tag{33}$$

Similar to last equation, we can expand electromagnetic wave to

$$H_{\vec{k}}(\vec{r}) = e^{i(\vec{k}.\vec{r})} \bullet u_{\vec{k}}(\vec{r})$$

(34)

Now Equation (11) can be expressed as

$$(i\vec{k} + \nabla) \times (\frac{1}{\varepsilon(\vec{r})}(i\vec{k} + \nabla)) \times u_{\vec{k}} = (\frac{w}{c})^2 u_{\vec{k}} = \bar{w}^2 u_{\vec{k}} \qquad (35)$$

and this is the fundamental equation of 'Plane Wave Expansion method'. For each k, Eq.(35) has an infinite number of solution $\bar{w}_{k,n}$ labeled by the band number, n, in order of increasing frequency. When we vary k over all possible values, the set of solutions $\bar{w}_{k,m}$ for a fixed integer m make a band, and the band structure is the collection of all these bands.

4.1 Design of photonic crystal resonant cavity

From Fig.3.2, our structure ground state emission wavelength is located at 1μm, so the band gap range we design must include this wavelength. At first, we calculate the band gap with the 2D photonic crystal slab without defect. As mentioned in chapter 2-4, we should keep in mind that effective reflective index has to be used instead of bulk refractive index, 3.42 when executing 2D simulation. From Fig.4.1, the band gap range is pulled down as effective refractive index increases. Besides, various r/a (r is hole's radius and a is lattice constant) ratios also modify band gap range due to variational principle, illustrated in Fig.4.2.

Now we introduce variational principle briefly. Analog to variational theorem of quantum mechanisms, there is also a variation principle in

electromagnetics. Namely, the smallest eigenvalue, $\frac{w_0^2}{c^2}$, and thus the lowest

frequency mode, correlates to the field pattern which minimize the function:

$$U_f(H) \triangleq \frac{(H, \hat{\Theta} H)}{(H, H)} \qquad (36)$$

If $U_f(H)$ is the minimum value of the lowest frequency mode, the small

energy change should be zero when adding small perturbing term $\delta H(r)$ to

$H(r)$. Here we access the energy function at $H + \delta H$ and at H. Then Eq.(12)

becomes

$$U_f(H + \delta H) = \frac{(H + \delta H, \hat{\Theta} H + \Theta \hat{\delta} H)}{(H + \delta H, H + \delta H)} \qquad (37)$$

Subtracting Eq.(12) from Eq.(13), we get

$$\delta U_f(H) \triangleq U_f(H + \delta H) - U_f(H) \qquad (38)$$

$\delta U_f(H)$ could be written in the form $\delta U_f(H) \approx [(\delta H, G) + (G, \delta H)]/2$ if we

ignore terms higher than first order in δH, where G is equal to

$$\frac{2}{(H, H)}(\hat{\Theta} H - [\frac{(H, \hat{\Theta} H)}{(H, H)}]H) \qquad (39)$$

We can think G as the gradient of $U_f(H)$. At the extreme, δU_f should

vanish for all possible shifts δH and thus G=0. This implies the parenthesized

quantity of Eq.(15) is also zero. That is, H is an eigenvector of $\hat{\Theta}$.

Consequently U_f is at an extreme if and only if H is a harmonic mode. Now if

we rewrite Eq.(12) by transferring H to E, and then Eq(12) becomes

$$U_f(H) = \frac{(\nabla \times E, \nabla \times E)}{(E, \varepsilon(r)E)} = \frac{\int |\nabla \times E(r)|^2 \, d^3 r}{\int \varepsilon(r) |E(r)|^2 \, d^3 r} \qquad (40)$$

Obviously the electric field should be concentrated on high dielectric region to minimize $U_f(H)$.

Due to variational principle, we observe that the larger the r/a ratio is, the higher frequency of band gap range is. Now we introduce a point defect and change neighboring six holes shapes and positions [25], like Fig.4.3. Neighboring six holes are shifted radially and shrunk to make radius, r', plus shift distance equal to radius, r. Fig.4.4 shows the top view of our structure of SEM picture. Since it's very essential for us to put the localized mode in the middle of band gap which makes parallel confinement best, we select lattice constant to be approximately 380nm and r/a ratio to be 0.36. The band diagram is shown in Fig.4.5. For more prudence we confirm our simulation is precise by Fig.4.6, Fig.4.7 and Fig.4.8. Here we require introducing a concept for a while. Again according to variational principle, a mode inclines to concentrate its electric-field energy in regions of high dielectric constant, while remaining orthogonal to the mode below its frequency. Therefore, when air hole areas increase, band gap range shifts to higher frequency region. In Fig.4.6, central wavelength of cavity mode becomes longer as period of air holes of photonic crystal increases which represents air hole proportion reduces. Fig.4.7 depicts when radius of neighboring six holes decreases, energy of cavity mode also becomes smaller, in other word, central wavelength of cavity mode moves toward longer wavelength. From Fig.4.8, if radius of air hole increases, that is, air hole area enlarges and then air hole portion is larger, central wavelength of cavity mode has "blue-shift" characteristic. In conclusion, we observe this trend from Fig.4.6 to 4.8.

Due to lithography resolution, in practice, we design the lattice constant varies from 370nm to 390nm and radius, r, (excludes six neighboring six holes) alters from 100nm to 120 nm. Finally six neighboring six holes adjust their radius, r', to make r'/r ratio from 0.6 to 0.9.
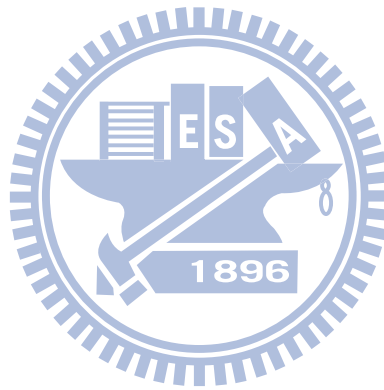
Fig.4.1 Frequency versus effective reflection index
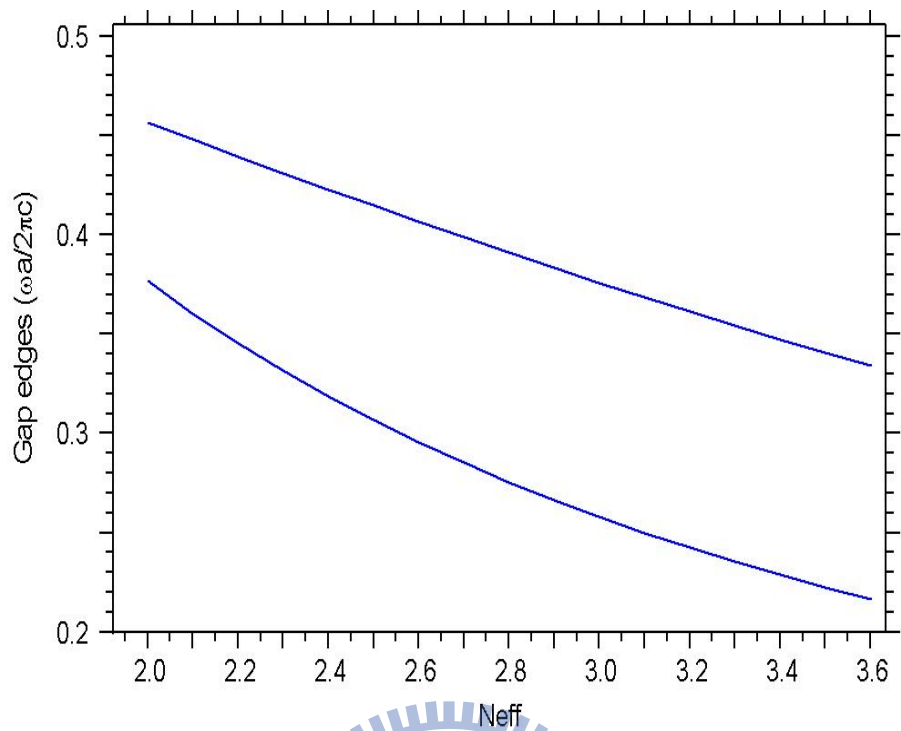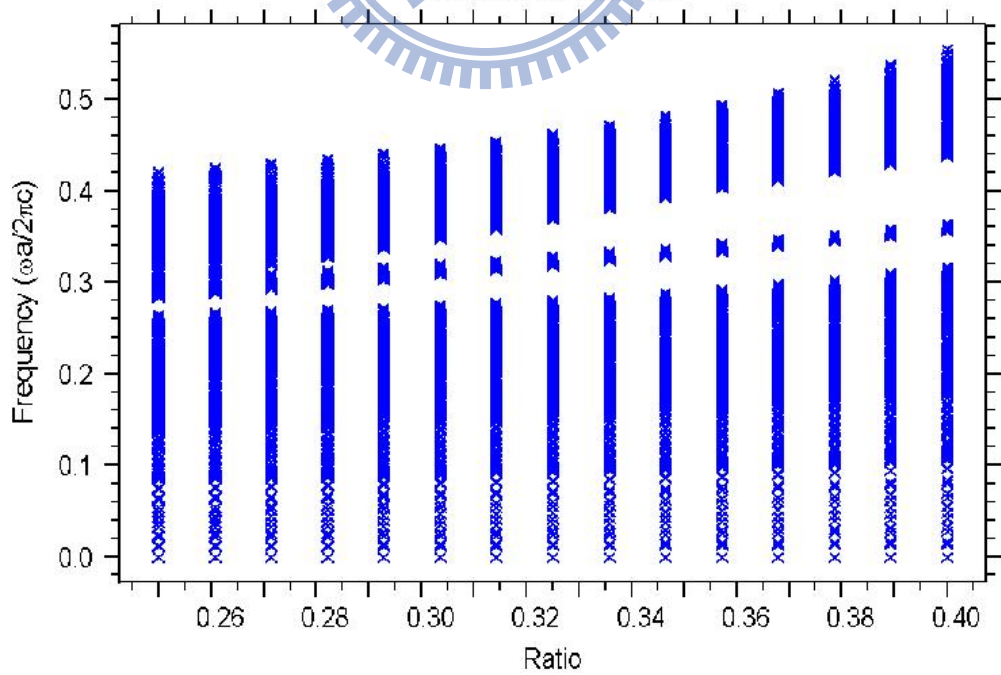

Fig.4.2 Frequency versus r/a ratio (r: radius, a: lattice constant)

(There is a defect mode in the middle of band gap)

Fig.4.3 Six neighboring holes varies shape and position

Fig.4.4 SEM picture of defect region

Fig.4.5 Band gap for photonic crystal with effective refractive index

Fig.4.6 Wavelength v.s. Lattice constant
(variational principle verification I)

Fig.4.7 Wavelength v.s. r'/r ratio
(variational principle verification II)

Fig.4.8 Wavelength v.s. r/a ratio for constant a
(variational principle verification III)

4-2　The value of Quality Factor of each resonant cavity

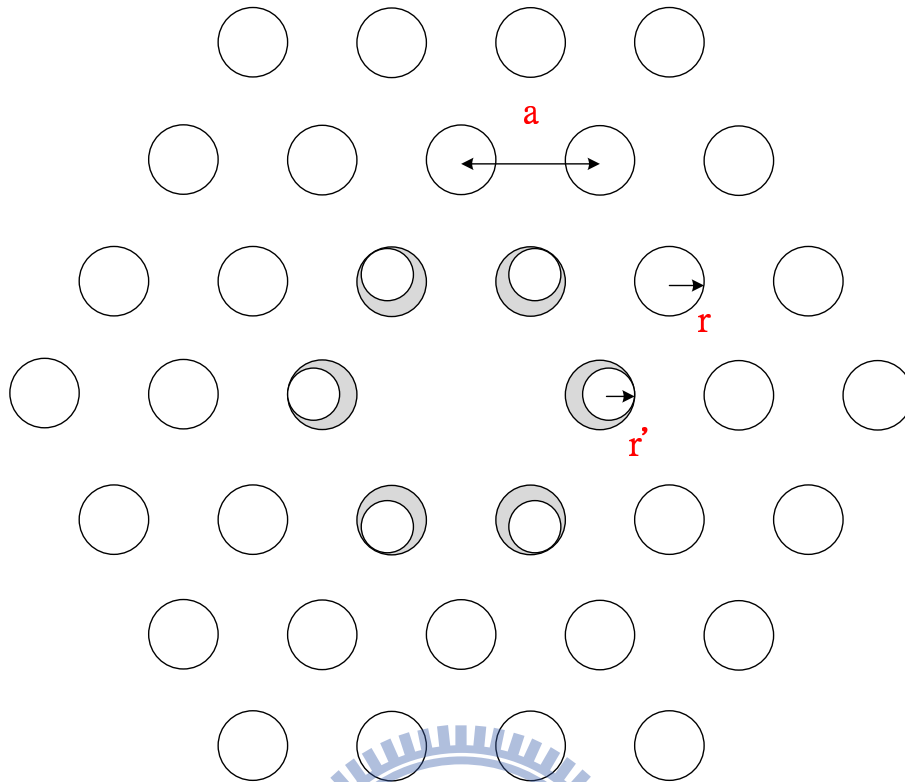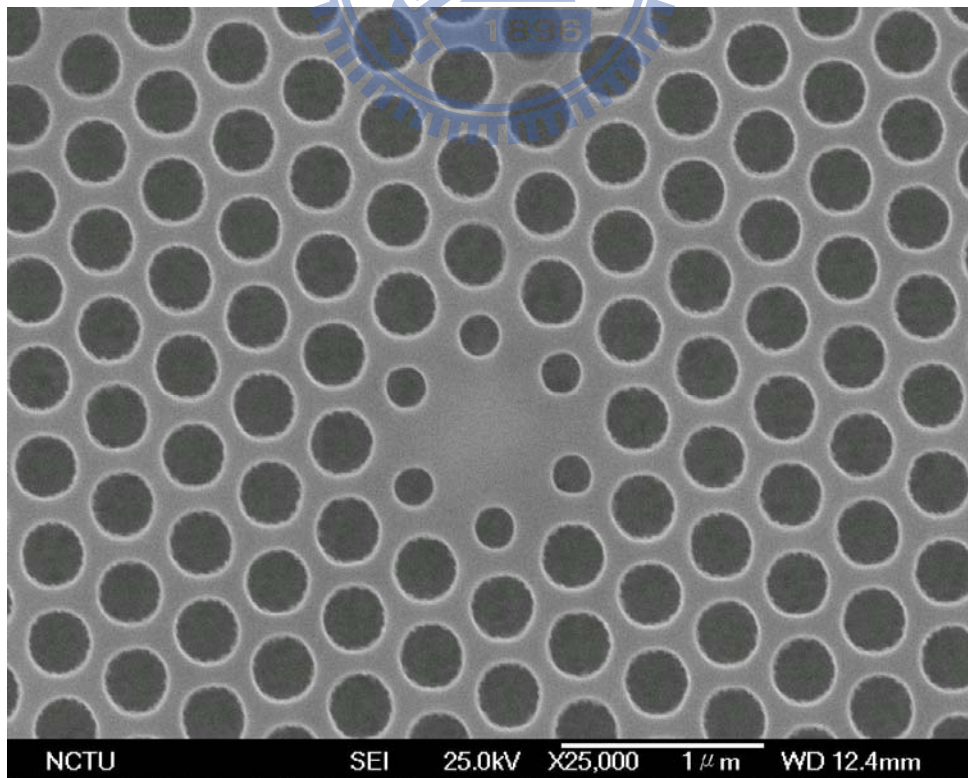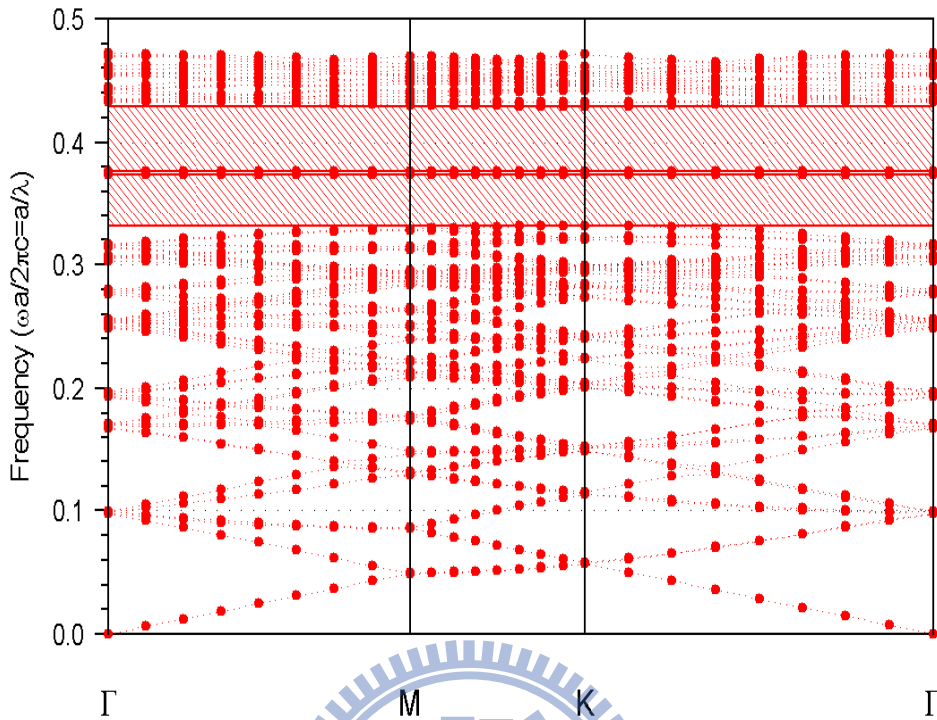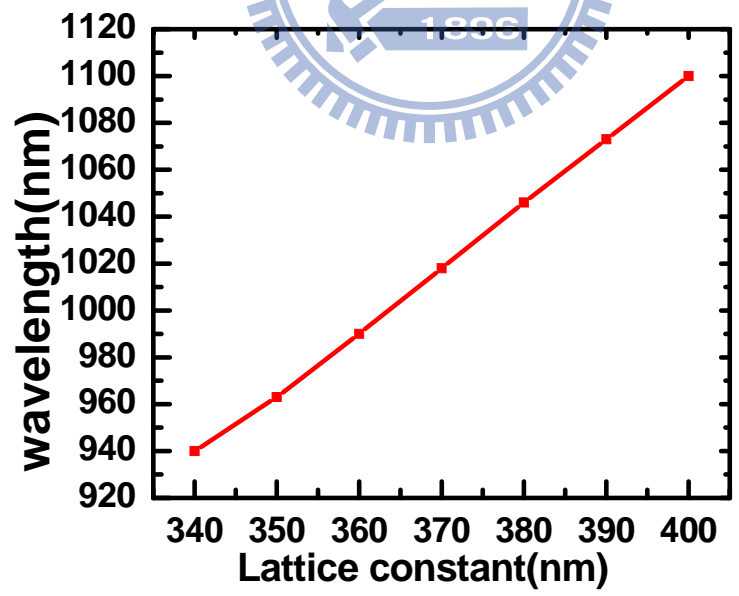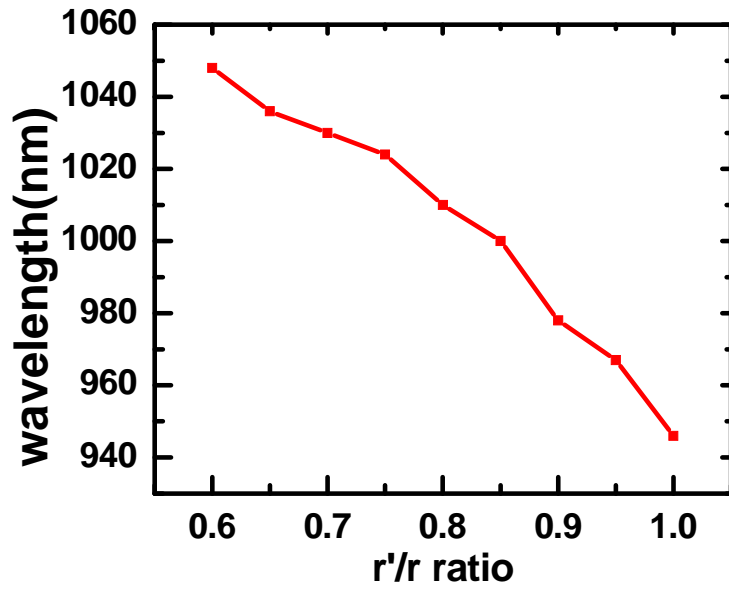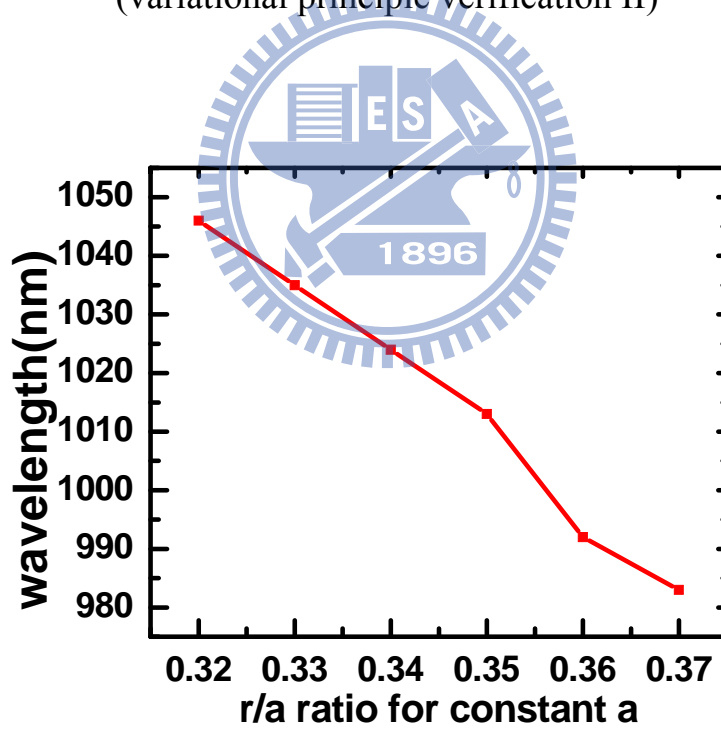In chapter 2-4, we mention the effective reflective index in order to save simulation time when calculating band diagram and resonant mode. For calculation of quality factor, however, 3D FDTD simulation is required since vertical quality factor ($Q_{vertical}$), neglected in 2D simulation, is dominated.

3D FDTD method, published by Yee, 1966 [26], describes electromagnetic distribution by numerical calculation. In chapter 2.2, we assume that there is no free charge and no current in our sample, so Maxwell curl equations written in Cartesian coordinates as six scalar equations becomes

$$\frac{\partial H_x}{\partial t} = -\frac{1}{\mu}(\frac{\partial E_z}{\partial y} - \frac{\partial E_y}{\partial z}) \tag{41}$$

$$\frac{\partial H_y}{\partial t} = -\frac{1}{\mu}(\frac{\partial E_x}{\partial z} - \frac{\partial E_z}{\partial x}) \tag{42}$$

$$\frac{\partial H_z}{\partial t} = -\frac{1}{\mu}(\frac{\partial E_y}{\partial z} - \frac{\partial E_x}{\partial y}) \tag{43}$$

$$\frac{\partial E_x}{\partial t} = \frac{1}{\varepsilon}(\frac{\partial H_z}{\partial y} - \frac{\partial H_y}{\partial z}) \tag{44}$$

$$\frac{\partial E_y}{\partial t} = \frac{1}{\varepsilon}(\frac{\partial H_x}{\partial z} - \frac{\partial H_z}{\partial x}) \tag{45}$$

$$\frac{\partial E_z}{\partial t} = \frac{1}{\varepsilon}(\frac{\partial H_y}{\partial z} - \frac{\partial H_x}{\partial y}) \tag{46}$$
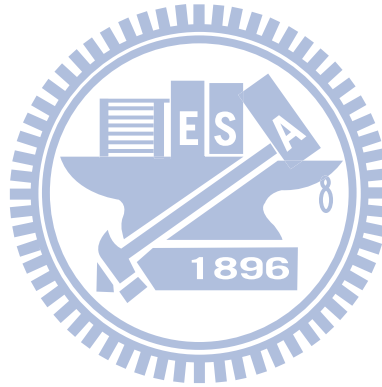
From these equations, the temporal electric field is dependent upon the spatial variation of magnetic field and vice versa. FDTD method solve Maxwell equation by discretizing the equations via central differences in time and space and then solving these equations numerically.

Based on Yee's lattice, electric and magnetic field components are computed at the point on a grid with grid spaced, $\Delta x, \Delta y, \Delta z$, shown in Fig.4.9. Electric field components are solved at a given time and then magnetic field

components are solved at next given time. This process is repeated until the desired electromagnetic field is fully achieved.

By Yee' lattice, Eq.(41) & (44) could be re-written as

$$\frac{H_x^{t+1/2}(i, j+\frac{1}{2}, k+\frac{1}{2}) - H_x^{t-1/2}(i, j+\frac{1}{2}, k+\frac{1}{2})}{\Delta t} = \frac{1}{\mu} \left\{ \frac{E_y^t(i, j+\frac{1}{2}, k+1) - E_y^t(i, j+\frac{1}{2}, k)}{\Delta z} - \frac{E_z^t(i, j+1, k+\frac{1}{2}) - E_z^t(i, j, k+\frac{1}{2})}{\Delta y} \right\}$$

$$\frac{E_x^t(i+\frac{1}{2}, j, k) - H_x^{t-1}(i+\frac{1}{2}, j, k)}{\Delta t} = \frac{1}{\varepsilon} \left\{ \frac{H_z^{t-1/2}(i+\frac{1}{2}, j+\frac{1}{2}, k) - H_z^{t-1/2}(i+\frac{1}{2}, j-\frac{1}{2}, k)}{\Delta y} - \frac{H_y^{t-1/2}(i+\frac{1}{2}, j, k+\frac{1}{2}) - H_y^t(i+\frac{1}{2}, j, k-\frac{1}{2})}{\Delta z} \right\}$$

the other four are symmetric equivalents of the above.

$Q = \frac{2\pi v}{\alpha}$, where v is resonant frequency of cavity and α is decay constant of stored energy, $U(t) = U_0 \exp(-\alpha t)$ is used to calculate quality factor. Fig.4.10 shows the quality factor with varied r'/r ratio. Here we find that there is a maximum Q value when r'/r is equal to 0.8.
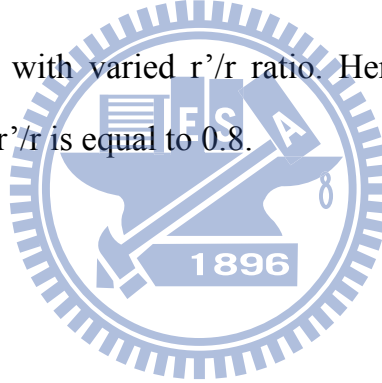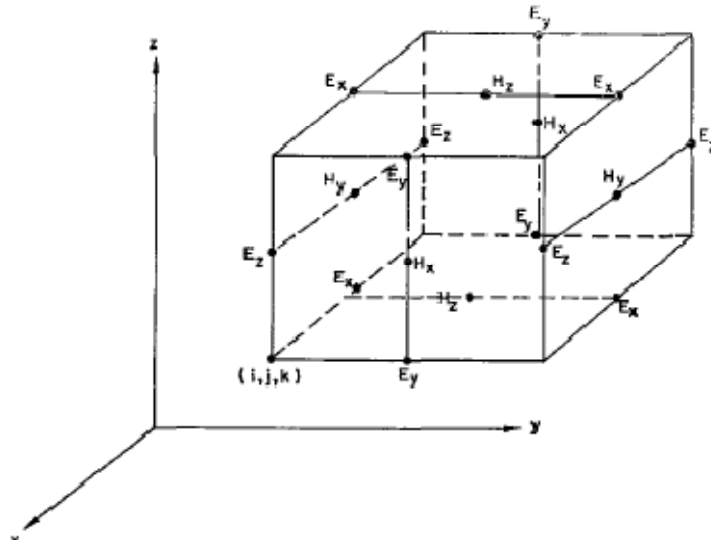
Fig.4.9 Three-dimensional Yee's lattice[26]
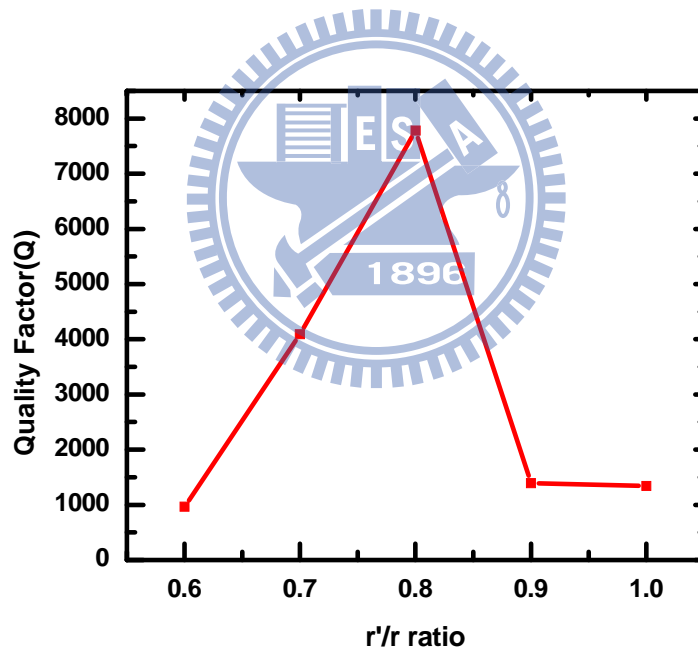
Fig.4.10 Total quality factor of varied r'/r ratio, where r is the hole radius
and r' is radius of the neighboring six holes of defect

4-3   Experiment measurements and discussion

From Fig.3.2, the emission central peak is around at 1um and full width at half maximum (FWHM) is equal to 54nm. That is, the total emission range is from 950nm to 1050nm (the main emission range, where emission intensity value is larger than half of maximum intensity value, is from 973nm to 1027nm). Compared to the simulation, Fig.4.11, there is only one cavity mode within the emission region and its position is at 1008nm. Another nearest cavity mode wavelength, out of emission range of the sample, is located at 923nm. Back to our measurement, here the cavity mode for photonic crystal lattice constant, a=375nm, radius r=130nm, and neighboring six holes radius r'=0.7r (Fig.4.12) and r'=0.8r (Fig.4.15) are acquired respectively by using measurement system introduced above. Here the external incident laser power 3mW is selected and beam spot diameter is approximately 3 um, so power density is about 10^4 W/cm^2. In Fig.4.12, the cavity mode for r'=0.7r is located at 1005nm as spectrum interval is 1nm and only this cavity mode is measured, corresponding to our simulation. Next we want to determine Q value of this cavity mode, so the small spectrum interval measurement is demanded; otherwise, the value of quality factor, $Q = \dfrac{\lambda}{\Delta\lambda(half\ \max)}$, is dramatically reduced and obviously inaccurate due to spectrum interval limitation. From Fig.4.13, with interval 0.01nm, the central wavelength of the cavity mode is at about 1003.08nm. In Fig.4.13, except main peak at 1003.08nm, there are many peaks which may results from noise signal perturbation. Increase signal/noise ratio by rising incident power intensity can make noise peak weaker relatively. Although there is a slightly wavelength difference between Fig.4.12 and Fig.4.13, the central wavelength of Fig.4.13 is much adequate owing to its

smaller interval. We can obtain the width of wavelength at half maximum of peak wavelength ($\Delta\lambda$) by Lorentz fitting and then $\Delta\lambda$ is equal to 0.08nm, shown in Fig.4.14. Using the formula, $Q = \dfrac{\lambda}{\Delta\lambda(half\ \max)}$, we find the quality factor of this cavity mode is about 15170. Lorentz distribution [18], a continuous probability distribution, is relevant since it is the solution to the differential equation describing resonance. Lorentz function could be expressed as

$$L(\lambda;\lambda_0;\Delta\lambda;I) = I[\frac{\Delta\lambda^2}{(\lambda - \lambda_0)^2 + \Delta\lambda^2}] \tag{47}$$

where I is the height of the peak.

Fig.4.15 shows the cavity mode for r'=0.8r, the central wavelength is approximately at 1003nm. Again only one cavity mode is measured. Compare with Fig.4.12 and Fig.4.15, the cavity mode for r'=0.8r has a higher Q value than r'=0.7r because the full-width-half maximum (FWHM) of the peak is narrower, where the trend is the same as our simulation. (Normally Q value of simulation is higher than measurement, but it's opposite in our case since the grid of simulation is not small enough to calculate correct quality factor value) Additionally, we observe that the central wavelength of r'=0.7r is longer than r'=0.8r, which is satisfied the variational principle: central wavelength of cavity mode shifts to longer wavelength as air hole portions reduces.
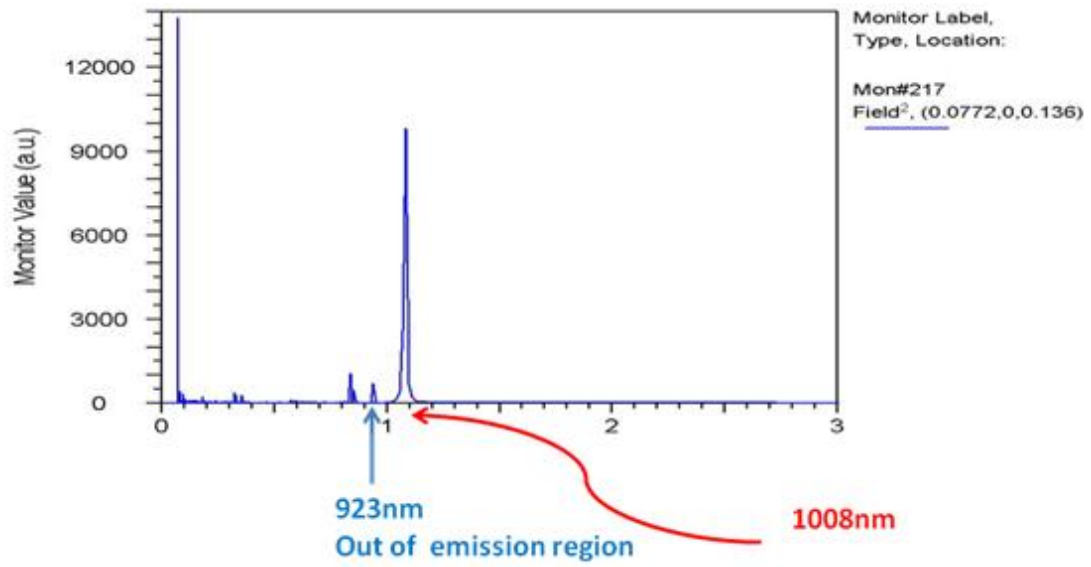
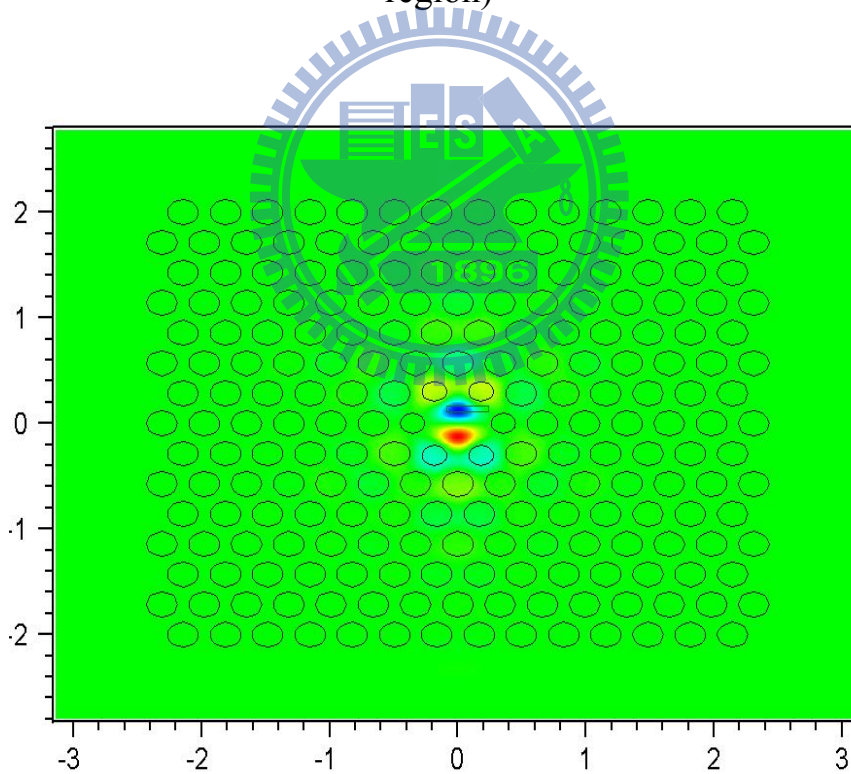Fig.4.11 Simulation of the cavity mode (only 1008nm peak with emission region)

Fig.4.12 Dipole mode of the cavity mode which is within emission region
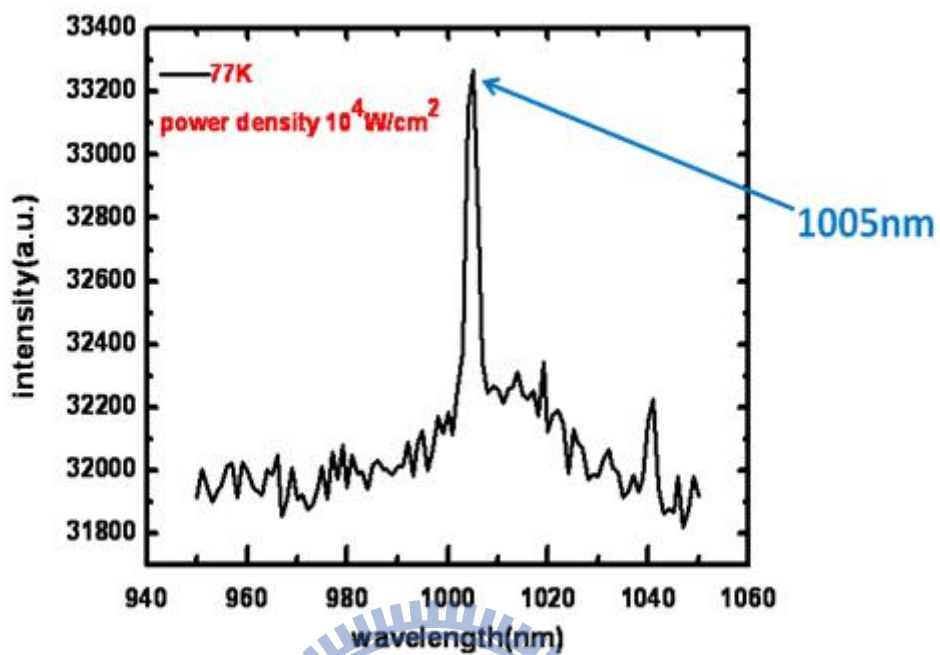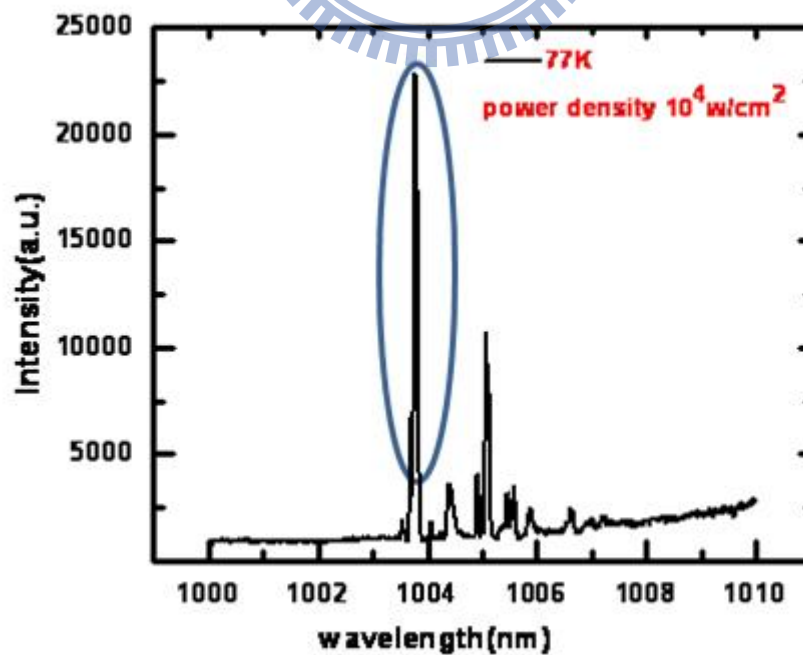
Fig.4.13Cavity mode for r'=0.7r (spectrum interval is 1nm)

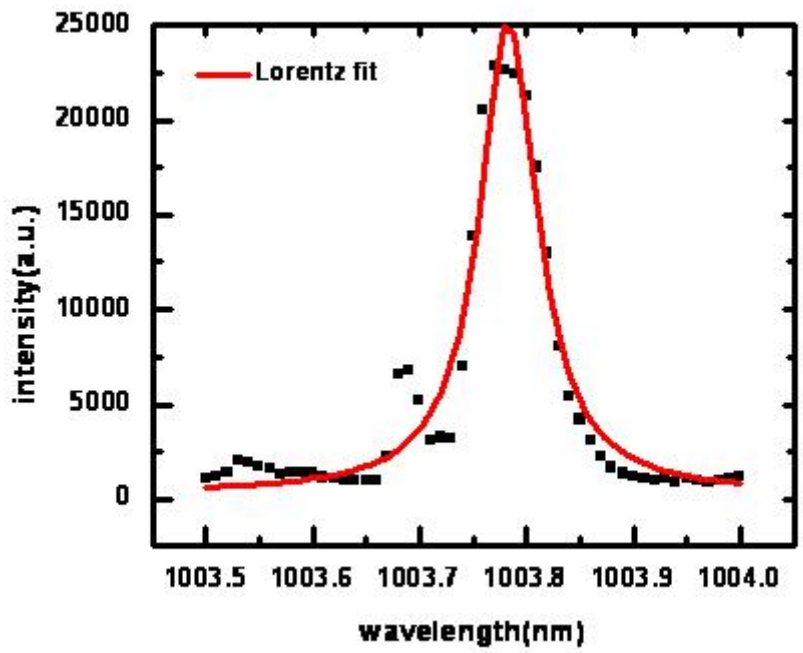Fig.4.14 Cavity mode for r'=0.7r (spectrum interval is 0.01nm)
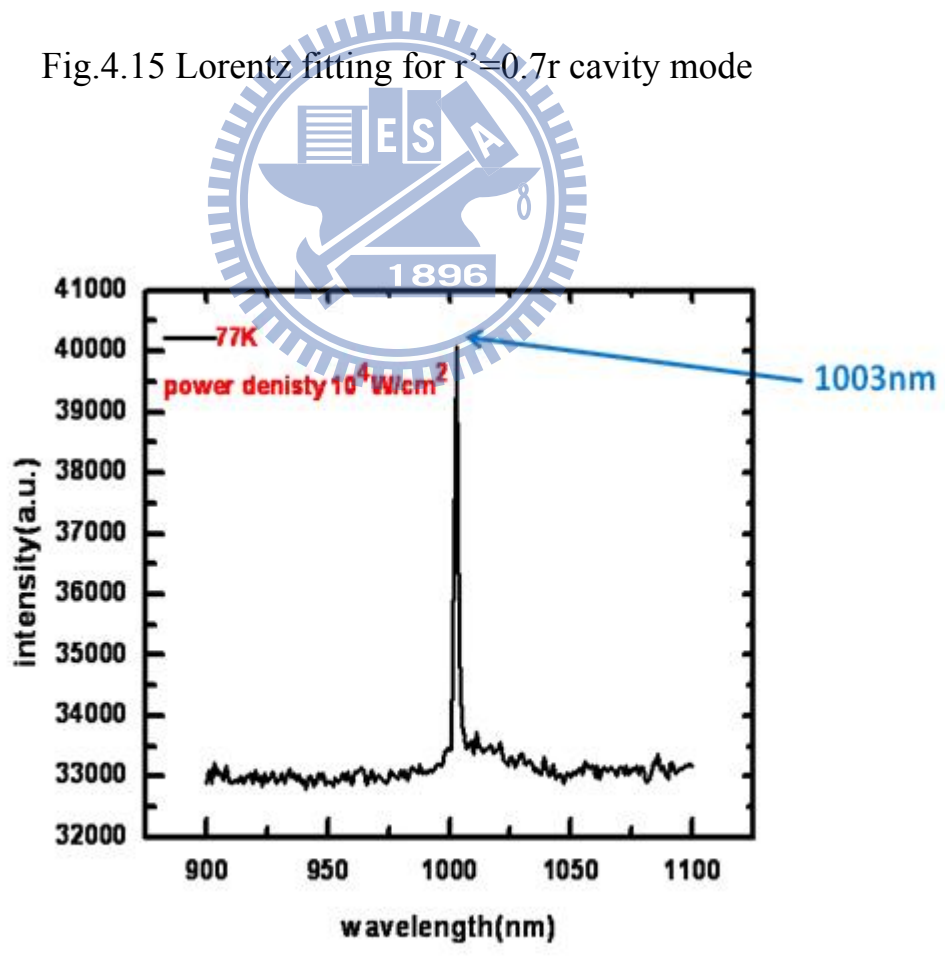
Fig.4.15 Lorentz fitting for r'=0.7r cavity mode

Fig.4.16Cavity mode for r'=0.8r (spectrum interval is 1nm)

Chapter 5 Conclusions and future works

2D photonic crystal membrane with a point defect inhibiting light propagation in horizontal direction could be used as resonant micro-cavity, which leads to small mode volume and high quality factor value merits. Type II GaAsSb/GaAs quantum well structure is profitable to 1.3 μ m emission wavelength with less attenuation characteristic.

In this thesis, type II GaAsSb/GaAs tri-quantum well layers with photonic crystal structure are successfully fabricated by molecular beam epitaxy, e-beam lithography and relative ion etching (RIE) technology. The total process flow is introduced in detail in chapter 3.2. We design 'wet etching window' at both sides of photonic crystal pattern to make wet etching process more smoothly and SEM observation more conveniently. In addition, the experimental condition of measurement system is described. Co-focal microscope and 100 magnification object lens are used so as to concentrate beam spot on micro-cavity region which is only 3-4 μ m^2. Also empirical temperature is 77K by liquid nitrogen cooling system since surface velocity, dominated mechanism of non-radiative recombination, of GaAs is 2*10^7 cm^2. To design appropriate photonic crystal pattern, 'Plane Wave Expansion method' is used to decide band gap range and cavity mode at the middle of band gap. In 2D simulation, instead of time-consuming 3D simulation, bulk refractive index must be replaced by effective refractive index because of the affection of surrounding air layer. Next various micro-cavity structures are designed: neighboring six holes of defect are shrunk and shifted at the same time to make six holes radius, r', plus shift distance, d, equal to other hole radius, r. The aim

to this design is that vertical quality factor, main mechanism of total quality factor, increases by changing neighboring six holes shapes and positions. Besides, according to variational principle, central wavelength of cavity mode will incline to shorter wavelength when air hole portions increases in order to maintain the lowest energy, we demonstrate this principle with our simulations, for instance, change hole radius, r, for a constant lattice constant. In 3D simulation, each quality factor values of various micro-cavity patterns are calculated and the quality factor value of neighboring six holes radius, r'=0.8r, is the highest. Finally cavity mode of our pattern was measured. The emission range of our type II GaAsSb/GaAs quantum well is from 950nm to 1050nm. In terms of simulation, only one cavity mode is located within the emission range, same as the measurement. The highest two quality factors of different cavity structures were measured. For cavity with r'=0.7r, the central wavelength of cavity mode was 1003.08 nm and $\Delta\lambda(half \max)$ was 0.08 nm by Lorentz fitting. That is, the quality factor of this cavity mode, up to 15000, was achieved. To our knowledge, this is the first time that a type-II heterstructure emission was coupled to a photonic nanocavity with a very sharp emission and a high Q value. Besides, the quality factor of cavity with r'=0.8r was higher than that of cavity with r'=0.7r since $\Delta\lambda(half \max)$ of cavity with r'=0.8r was narrower than cavity with r'=0.7r, corresponding to our simulation. Moreover, central wavelength of cavity with r'=0.8r was shorter than r'=0.7r, which is satisfied with variational principle. Basis on our experimental results, it is promising for 1.3 μ m laser source.

In order to develop 1.3 μ m laser, in the experiment, exciting another cavity mode with higher quality factor value, like quadrapole or hexapole, is

necessary for low threshold current. Besides, the value of x of GaAs$_x$Sb$_{1-x}$/GaAs is needed to make some adjustment to accomplish 1.3 μm emission. In measurement system, pulse laser source with high power is needed since thermal effect is serious due to surrounding air layer which thermal conduction coefficient is very low. Besides, TRPL can measure life time of excited photon and polarizer measurement can ensure which kind of pole of cavity mode is excited. Finally, it's hopeful to realize laser source by electric pumping.

Reference

[1] Andrew S. Tanenbaum, "Computer Networks", Upper Saddle River, N.J.

Prentice Hall PTR, 1996

[2] V. Swaminathan, "Material Aspects of GaAs and InP Based Structures",

Prentice-Hall, Inc., 1991

[3] E. Yablonovitch, "Inhibited Spontaneous Emission in Solid-State Physics and

Electronics", Phys. Rev. Lett. **58**, 2059, 1987.

[4] S. John, "Strong localization of photons in certain disordered dielectric

superlattices", Phys. Rev. Lett. **58**, 2486, 1987.

[5] O. Painter et al., "Two-dimensional photonic band-gap defect mode Laser,"

Science **284**, 1819, 1999

[6] Yoshihiro Akahane et al., "High-Q photonic nanocavity in a two-dimensional

photonic crystal" Nature **425**, 944, 2003

[7] K. Noazki et al. "Laser characteristics with ultimate-small modal volume in

photonic crystal salb point-shift nanolasers", Appl. Phys. Lett, **88**, 211101, 2006

[8] T. Anan et al, "GaAsSb: A novel material for 1.3μm VCSELs," Electronics Lett.

34, 2127, 1998

[9] O. Blum and J. F. Klem, "Characteristics of GaAsSb single-quantum-well-lasers

emitting near 1.3μm," IEEE Photonics Tech. Lett.**12**, 771,2000

[10] S. W. Ryu and P. D. Dapkus, "Low threshold current density GaAsSbquantum

well lasers grown by metal organic chemical vapor deposition on GaAs substrates,"

Electronics Lett. **36**, 1387,2000

[11] P.-W. Liu, G.-H. Liao and H.-H. Lin, "1.3 lm GaAs=GaAsSb quantum well

laser grown by solid source molecular beam epitaxy", Electronics Lett. 40, 177, 2004

[12] T.Anan et al, "Room-temperature pulsed operation of GaAsSb/GaAs

vertical-cavity surface emitting lasers", Electronics Lett. **35**, 903, 2001

[13] F. Quochi et al, "Continuous-Wave Operation of a 1.3-μm GaAsSb–GaAs Quantum-well vertical-cavity surface-emitting Laser at room temperature", IEEE Photonic Tech Lett. **13**, 921, 2001

[14] T.Baier et al, "Type-II band alignment in $Si/Si_{1-x}Ge_x$ quantum wells from photoluminescence line shifts due to optically induced band-bending effects: Experiment and theory", Physics Review B **50**, 15190, 1994

[15] W.W. Chow, H.C. Schneider, "Charge-separation effects in 1.3 mm GaAsSb type-II quantum-well laser gain", Appl. Phys. Lett. **78**, 4100, 2001

[16] D.S. Jiang et al., "Structural and optical properties of GaAsSb/GaAs heterostructure quantum wells", Journal of Crystal Growth **268**, 336, 2004

[17] Y. S. Chiu et al "Properties of photoluminescence in type-II GaAsSb/GaAs multiple quantum wells", Journal of Applied Physics **92**, 5810, 2002

[18] John. D. Joannopoulos, Robert D. Meade, and Joshua N. Winn, <u>Photonic crystals: molding the flow of light, 2nd</u>, New Jersey, 2008

[19] Fujita, M. et al., "Simultaneous inhibition and redistribution of spontaneous light emission in photonic crystals", Science **308**, 1296, 2005

[20]K. Kounoike et al., "Investigation of spontaneous emission from quantum dots embedded in two-dimensional photonic-crystal slab", Electronics Letters **41,** 1402, 2005

[21] Hong-Gyu Park et al., "Characteristics of Modified Single-Defect Two-Dimensional Photonic Crystal Lasers", IEEE Journal of Quantum Eelctronics **38**, 1353, 2002

[22] N. Carlesson et al., "Design, nano-fabrication and analysis of near-infrared 2D photonic crystal air-bridge structures", Optical and Quantum Electronics **34**, 123, 2002

[23] Jong-Hee Kim, Dae Ho Lim, and Gye Mo Yang, "Selective etching of AlGaAs/GaAs structures using the solutions of citric acid/H2O2 and de-ionized H2O/buffered oxide etch", J. Vac. Sci. Technol. B **16**, 558, ,1998"

[24] K. Sakoda, Optic Properties of Photonic Crystals, Springer, 2001

[25] D. G. Gevaux et al., "Enhancement and suppression of spontaneous emission by temperature tuning InAs quantum dots to photonic crystal cavities", Appl. Phys, Lett. **88**, 131101, 2006

[26] K.S. Yee, 'Numerical solution of initial boundary value problems involving maxwell's equations in isotropic media,' IEEE Trans. Antennas Propag. , **14**, 302, 1966

Autobiography(自傳)

姓名:林俊豪(Lin,Chun-Hao)

性別:男

出生年月日:民國 74 年 8 月 24 日

學歷:

國立交通大學電子工程學系(92.9-96.6)

國立交通大學電子工程研究所碩士班(96.9-98.10)

碩士論文題目:

利用光激發於結合光子晶體的類型二量子井之研究

Study of Type II QW with photonic crystal structure by optical Pumping